International Journal of Pharmaceutics 677 (2025) 125514

Contents lists available at ScienceDirect

International Journal of Pharmaceutics

journal homepage: www.elsevier.com/locate/ijpharm

Injectable anticancer biodegradable hydrogel-based nanocomposites: Synergistic pH-responsive paclitaxel/β-cyclodextrin nanocomplex delivery in polyvinyl alcohol hydrogel for targeted pancreatic ductal adenocarcinoma treatment

Xiuxiu Li [a], Weiyu Ma [a], Zhou Xu [a,*], Ninggang Zhang [a,*], Shubham Sharma [b,c,d], T. Ramachandran [e], A. Karthikeyan [f,1], Dhirendra Nath Thatoi [g,2], AI Ismail [h]

[a] Department of Gastroenterology, Shanxi Province Cancer Hospital, Shanxi Hospital Affiliated to Cancer Hospital Chinese Academy of Medical Sciences, Cancer Hospital Affiliated to Shanxi Medical University, No.3, Xinghualing District, Taiyuan, Shanxi 030001, China
[b] Department of Technical Sciences, Western Caspian University, Baku, Azerbaijan
[c] Centre for Research Impact and Outcome, Chitkara University Institute of Engineering and Technology, Chitkara University, Rajpura 140401 Punjab, India
[d] Jadara University Research Center, Jadara University, Jordan
[e] Department of Mechanical Engineering, School of Engineering and Technology, JAIN (Deemed to be University), Bangalore, Karnataka, India
[f] Department of Mechanical Engineering, Sathyabama Institute of Science and Technology, Chennai, Tamil Nadu, India
[g] Department of Mechanical Engineering, Siksha 'O' Anusandhan (Deemed to be University), Bhubaneswar, Odisha 751030, India
[h] Mechanical Engineering Department, College of Engineering and Architecture, UMM Alqura University, Saudi Arabia

A R T I C L E I N F O

Keywords:
Pancreatic ductal adenocarcinoma
Paclitaxel
β-cyclodextrin
Injectable hydrogels

A B S T R A C T

Pancreatic ductal adenocarcinoma (PDAC) is a cancer that is highly aggressive and has a challenging tumor microenvironment, which restricts the efficacy of conventional medical treatments. This investigation aims to formulate a localized anticancer hydrogel that incorporates a Paclitaxel/β-cyclodextrin (β-CD) nanocomplex composed of polyvinyl alcohol (PVA). Enhancements in drug delivery, therapeutic efficacy, adverse effects, and the mitigation of multidrug resistance are the objectives of PDAC treatment. In silico analyses were performed to examine the interaction between paclitaxel (PTX) and β-CD, which revealed favorable binding and pH-dependent release characteristics. Via FTIR and XRD analyses, the PTX/β-CD inclusion complex was verified. A hydrogel based on PVA was subsequently formed by incorporating this complex. The hydrogel's physicochemical and structural characteristics were examined using SEM, FTIR, XRD, and rheological methods.. Hydrogel's physical characteristics were evaluated through biodegradation and water absorption experiments. The cytotoxic and anti-metastatic potential of the hydrogel nanocomposite was quantified by conducting MTT assays and invasion and migration assays to assess its anticancer efficacy. The estimated adsorption energy (Eads) of PTX within β-CD to form the PTX/β-CD complex was -1.133×10^{-3} kJ/mol. In the Monte Carlo (MC) method, van der Waals forces and electrostatic interactions were considered based on group-based interactions with a cutoff radius of 12.5 Å. The interaction energy of B and PVA on PTX/β-CD was −319.150 kJ/mol. The binding energy ($E_{binding} = E_{interaction}$) for B/PVA/PTX/β-CD was found to be −60.977 at pH 3.4 and −69.312 at pH 7.4. In acidic conditions, the Paclitaxel/β-CD nanocomplex exhibited efficient drug release and strong binding interactions. Biodegradation (80 % weight loss within 28 days) and water absorption (up to 500 % of its dried weight) were both exceptional characteristics of the PVA hydrogel. According to anticancer assays, the nanocomposite exhibited substantial cytotoxic effects, which included the inhibition of cancer cell migration and invasion. Paclitaxel's solubility and biological activity were significantly improved by the injectable hydrogel, which confirmed its potential as a sophisticated local drug delivery system.

* Corresponding authors.
E-mail addresses: lixiuxiu126@163.com (X. Li), maweiyu1280@163.com (W. Ma), xuzhouty2017@163.com (Z. Xu), zng1120@163.com (N. Zhang), shubham543sharma@gmail.com, shubhamsharmacsirclri@gmail.com (S. Sharma), t.ramachandran@jainuniversity.ac.in (T. Ramachandran), akarthikeyan.auto@sathyabama.ac.in (A. Karthikeyan), dhirendrathatoi@soa.ac.in (D.N. Thatoi), aiismail@uqu.edu.sa (A. Ismail).
[1] https://orcid.org/0000-0003-0435-9822.
[2] 0000-0002-2633-4805.

https://doi.org/10.1016/j.ijpharm.2025.125514
Received 25 January 2025; Received in revised form 6 March 2025; Accepted 22 March 2025
Available online 11 April 2025

Conclusions: For the localized treatment of PDAC, the PVA-based injectable hydrogel that has been developed, which includes a Paclitaxel/β-CD nanocomplex, is a promising approach. Its targeted delivery, enhanced solubility, and potent anticancer characteristics offer a valuable method for enhancing therapeutic outcomes while reducing systemic side effects and multidrug resistance.

1. Introduction

Pancreatic ductal adenocarcinoma (PDAC) is widely acknowledged as one of the most aggressive and fatal cancers, contributing substantially to cancer-related fatalities worldwide. With a remarkably high mortality rate, it is expected to rise to the second leading cause of cancer deaths in the coming decade (Chandana et al., 2019). PDAC originates in the pancreatic ducts and is characterized by its late presentation and rapid progression, often evading early detection due to vague symptoms (Kenner et al., 2021).

A hallmark of PDAC is its complex tumor microenvironment (TME), which features a dense stroma comprised of various fibroblasts, immune cells, and extracellular matrix components (Truong and Pauklin, 2021). This immunosuppressive microenvironment not only contributes to tumor growth and metastasis but also poses significant challenges to effective treatment, limiting the efficacy of conventional therapies such as chemotherapy and radiotherapy (Ho et al., 2020). Furthermore, the unique biological characteristics of PDAC, including its resistance to drug delivery and inherent genetic mutations, complicate the development of targeted therapeutic options (Liu et al., 2021).

In light of the pressing need for new and effective treatment options, research is increasingly focused on unraveling the molecular mechanisms of pancreatic ductal adenocarcinoma (PDAC) and investigating cutting-edge therapeutic approaches, including targeted drug delivery systems and innovative biomaterials (Ferrara et al., 2021). Developing promising therapeutic approaches is critical to improving patient outcomes and addressing the formidable challenges of this devastating disease (Chintamaneni et al., 2024).

The utilization of chemotherapy as a neoadjuvant strategy has demonstrated favorable outcomes in terms of the survival rates of individuals diagnosed with PDAC (Springfeld et al., 2023). Moreover, it has been noted to improve tumor-free survival rates and could make surgical intervention possible for patients considered initially unsuitable candidates for tumor removal (Seufferlein and Ettrich, 2019). Recent research findings have indicated that administering paclitaxel (PTX) can decrease tumor size and enhance surgical success rates while exhibiting minimal adverse effects (Bernabeu et al., 2017). As a result, this treatment approach shows potential for improving overall survival rates in patients diagnosed with PDAC. While significant progress has been made in treating specific tumors, the use of chemotherapy with PTX can lead to serious hypersensitive reactions. These adverse effects, including hematologic toxicity and neurotoxicity, may diminish the therapeutic benefits of PTX (Bernabeu et al., 2017; Wang et al., 2017).

Thus, creating new treatment strategies that reduce side effects is essential. However, one major hurdle with paclitaxel is its poor water solubility. The current approach to this challenge involves creating a complex between paclitaxel and β-Cyclodextrin (β-CD) (Bouquet et al., 2007).

β-CD is a cyclic oligosaccharide composed of seven D-glucopyranose units linked together through α-1,4 glycosidic linkages. They are highly biologically available, easily adaptable, have good solubility, and do not exhibit toxicity. Additionally, because of their unique cavity that may form reversible compounds with different medications, they can be used to create controlled release systems. Polymers, which comprise a three-dimensional network appropriate for drug delivery applications, can also be created by crosslinking CDs with bi- or multifunctional agents (Escobar et al., 2023).. CD-based drug delivery systems significantly improve drug stability and limit adverse effects in the body, producing a targeted, secure, and efficient medicine to lessen the occurrence of potential postoperative issues. These factors have led to the functionalization of several biological materials for drug release applications using CD-based polymers… The unique structural traits of β-CD molecules give them an outstanding ability to encapsulate hydrophobic substances within their interior cavity and dissolve them in water (Sahu et al., 2023).

Over the past few years, there has been a significant rise in attention towards injectable in situ hydrogels as promising platforms for drug delivery, particularly in the field of anticancer treatment (Zhao et al., 2022).

Hydrogels can transport a variety of treatments to treat diseases, such as proteins, nucleic acids, small molecule medicines, and cell preparations, because of their unique physical and chemical characteristics.

(Rizzo and Kehr, 2021). Hydrogels' high water content and porosity networks give them exceptional capabilities for effectively encasing both small- and large-molecule medications. Chemical and physical interactions can be used to load drugs into hydrogels. On the one hand, by blending directly with the hydrogel polymers, hydrophilic medications could be physically confined in hydrogels. In order to increase their water solubility, hydrophobic medications are frequently loaded into hydrophilic micro/nanoparticles, which further traps them inside the hydrogels. (HB et al., 2010).

In order to transport GEM nanoparticles and the PTT sensor DPP-BTz to the TME, Yingjie, Kong, and colleagues created an injectable thermosensitive hydrogel. In this work, thermosensitive liposomes loaded with GEM and a photosensitizer DPP-BTz were created using DPPC. Furthermore, thermosensitive hydrogels encasing the previously stated liposomes were prepared using PLEL. The hydrogel solution underwent a gelation process that was initiated by the mouse's body temperature after being injected into the tumor tissue of a murine PDAC model. The photosensitizer-mediated photothermal effect was then started by applying near-infrared light (1064 nm) in vitro. The structure of the thermosensitive liposomes was upset by this impact, which raised the local temperature and caused GEM to leak into the hydrogel. As a result, GEM spread across the TME and successfully caused PDAC cells to undergo apoptosis (Kong et al., 2021).

An ultrasound-responsive microbubble hydrogel was created by Huang, D. et al. to supply GEM and H_2S gas to PDAC TME simultaneously. They created a hydrogel precursor with an outer shell of alginate and PNIPAM filled with GEM and an inner core containing H_2S gas using microfluidic electrospray technology. UV light and calcium ions were used to crosslink the hydrogel precursor. When the hydrogels were injected into the mice's PDAC tissue, the H_2S gas inside the inner layer of the hydrogel expanded and oscillated due to in vitro ultrasonic stimulation, raising the ambient temperature. H_2S and water-soluble GEM were released into the surrounding tumor tissue as a result of the hydrogel's outer layer contracting simultaneously, which had an anticancer effect (Huang et al., 2021).

Considering the biological properties of pancreatic ductal adenocarcinoma and the pancreas's distinct anatomical features, we propose that a polyvinyl alcohol (PVA) hydrogel loaded with a Paclitaxel/β-cyclodextrin nanocomplex could be an effective in situ therapeutic approach for this type of cancer. PVA is a biocompatible, biodegradable, and FDA-approved polymer with promising potential for biomedical applications. PVA can form a 3D hydrogel with sodium tetraborate decahydrate(borax) at body temperature. Two neutral $B(OH)_3$ molecules and two $B(OH)_4^-$ ions (with counterion Na^+) can be formed by the hydration of the borax salt molecule, and the latter can complex with the

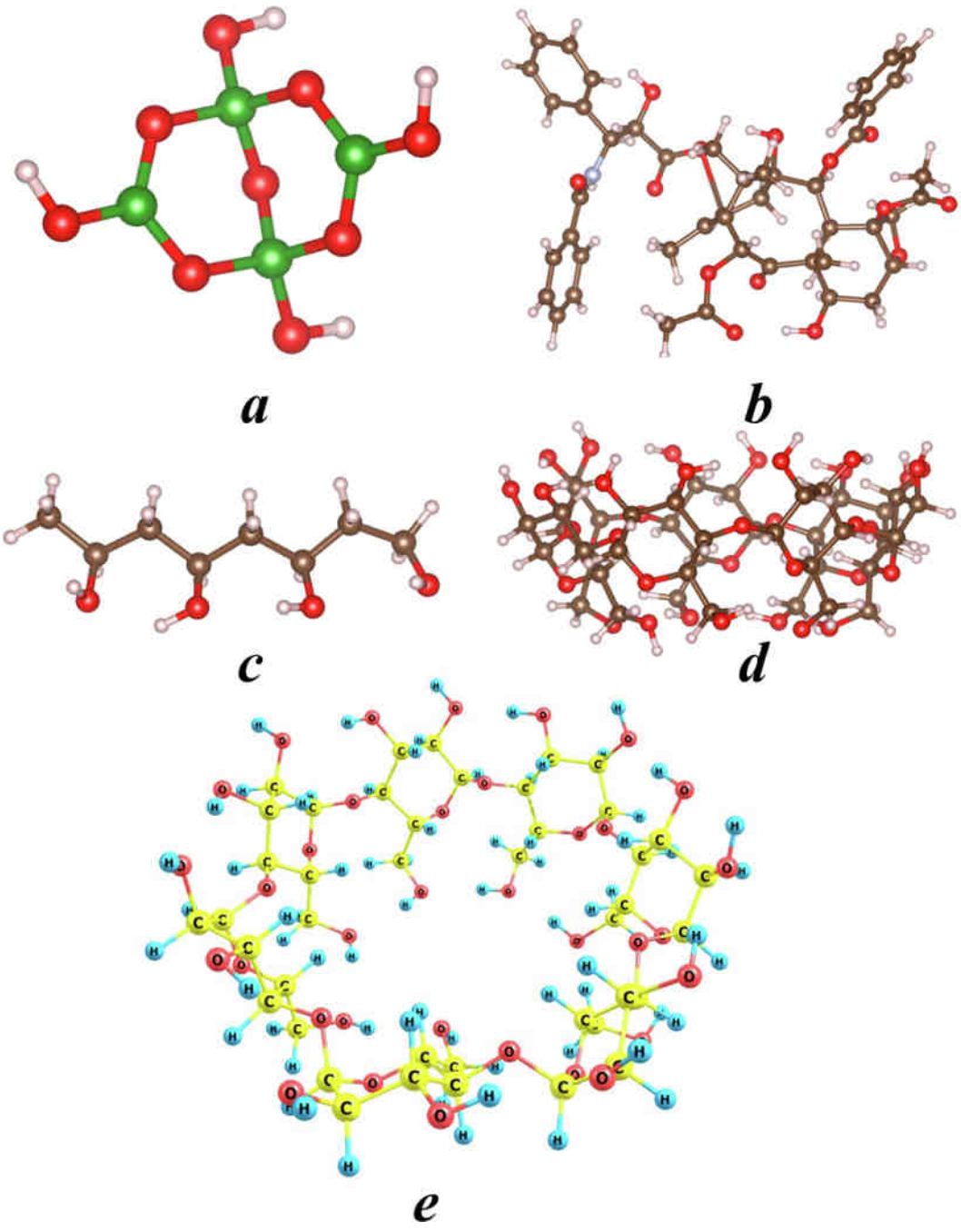

Fig. 1. The optimized structures of (a); borax, (b); Paclitaxel, (c); Polyvinyl alcohol and (d and e); the side views of β-cyclodextrin by using DFT-D method based on DMol (Truong and Pauklin, 2021) module in Material Studio 2017.

PVA chains. There are at least three distinct forms of $B(OH)_4^-$ for this model system, including the free $B(OH)_4^-$ and $B(OH)_4^-$ that form complexations with one or two sites (Li et al., 2018). In this study, we employed the PVA hydrogel composite in a pancreatic ductal adenocarcinoma model to assess the efficacy of the Paclitaxel/β-cyclodextrin nanocomplex in targeting tumors, as well as to explore its anticancer mechanisms in detail. The novelty of the present study is not only the complexation of paclitaxel and beta-cyclodextrins but also the inclusion of the complex into a hydrogel for local drug delivery application for targeted pancreatic ductal adenocarcinoma treatment, as well as conducting in silico simulations.

2. Experimentation: Materials and methods

2.1. Materials

In this research, β-CD, PTX, Borax, and PVA were obtained from Sigma Aldrich (USA), while DMSO and ethanol were prepared by Merck. All materials used were of analytical grade and were employed without further purification.

2.2. The in-silico optimization of PTX/β-CD and PTX/β-CD /PVA

2.2.1. DFT-D and Monte Carlo calculations

The dispersion corrections (DFT-D) approach calculates the long-range van der Waals interactions proposed by Grimme with spin-

unrestricted (Gholivand et al., 2023). To obtain the most stable structures, all structures were optimized based on DFT-D *via* DMol^3 package, Perdew–Burke–Ernzerh function (GGA–RPBE), and Basis set; DND; 3.5 to calculate their stable geometries (Gholivand et al, 2023). The optimized structures of the compounds, including Borax (B), Paclitaxel, polyvinyl alcohol (PVA), and β-cyclodextrin (β-CD), are shown in Fig. 1a-e. Finally, Monte Carlo simulations were conducted using the adsorption locator module with a universal forcefield to examine the adsorption interactions between the adsorbent and adsorbates at distances less than 10 Å (Gholivand et al., 2022).

2.3. Synthesis of Paclitaxel/β-cyclodextrin inclusion complexes

The following section describes the standard procedure for synthesizing inclusion complexes with PTX/β-CD (Song et al., 2016). First, an 86 mg (18.9444 mmol) sample of β-CD was dissolved in 4 mL of deionized water and mixed with a solution of paclitaxel (0.85 mg, 0.001 mmol)) in 4 mL of ethanol. This combination was stirred at room temperature in the dark for five days. Afterward, centrifugation was performed to remove any insoluble paclitaxel. The solvent was then evaporated under vacuum to reduce the volume to approximately 4 mL using a rotary evaporator. The resulting residue underwent another round of centrifugation to separate any precipitate. Finally, the remaining substance was lyophilized, yielding solid β-CD/PTX. The hydrogels were frozen for 24 h at − 80 °C and then the frozen samples were lyophilized for 48 h at − 54 °C. The lyophilized hydrogels were stored at −20 °C for further analysis and applications.

2.4. Characterizations of Paclitaxel/β-cyclodextrin via

2.4.1. Fourier transform infrared spectroscopy

The Fourier transform infrared (FT-IR) spectra of pure β-cyclodextrin, Pure PTX and the β-CD/PTX complex in potassium bromide (KBr) were obtained using a Shimadzu IRPrestige-21 spectrometer across the wavenumber range of 4000–400 cm^{-1}.

2.4.2. Ultraviolet–Visible spectroscopy

The UV–vis absorption spectra were obtained using a Shimadzu UV-2600 spectrophotometer. This was achieved by comparing with either a PBS blank or a 1:1 v/v combination of methanol and PBS. The absorbance of βCD at 2.0 mg/mL, βCD inclusion complexes at 2.0 mg/mL, and PTX at 0.02 mg/mL was determined utilizing quartz cuvettes with frosted walls, each having a volume of 0.7 mL.

2.4.3. Dynamic light scattering (DLS) measurement

The Zetasizer Nano ZS instrument from Malvern Instruments in Westborough, MA, was used to measure hydrodynamic size. It operated with a laser wavelength of 633 nm and a scattering angle of 173°. Solutions of the inclusion complexes were prepared by dissolving a fixed amount of complexes in phosphate-buffered saline (PBS). Measurements were carried out at temperatures of 25 °C and 37 °C. Before taking the measurements, the sample solution was equilibrated for 30 min at the designated temperature. The sensor provided average hydrodynamic diameters based on the particle distribution.

2.4.4. Scanning electron microscopy

Scanning electron microscopy (SEM) is a qualitative research technique employed to visually analyze the surface characteristics of an object. The standard error of the products was obtained using an environmental scanning electron microscope. Various freeze-dried inclusion complexes of βCD/PTX were examined, each coated with approximately 5 nm of platinum.

2.5. Fabrication process of polyvinyl alcohol hydrogel loaded with Paclitaxel/β-cyclodextrin nanocomplex

To prepare the hydrogels, start by dissolving 0.1 g of borax powder in aqueous solutions containing 1.0 percent of βCD/PTX inclusion complexes. Stir this mixture continuously at 25 °C for 20 min. Simultaneously and separately, the PVA solution was prepared by dissolving 0.5 g of PVA powder in 10 mL DI water and stirring for 2 h at 90 °C to obtain a clear solution. Then, the PVA solution was cold down to RT. Next, the cross-linker (Borax and βCD/PTX inclusion complexes) was added to the PVA solution under vigorous stirring. The solution was stirred for 24 h at RT. To remove any bubbles that may have formed during mixing, place the solutions in an ultrasonic water bath at 35 °C for 10 min.

2.6. Characterizations of polyvinyl alcohol hydrogel loaded with Paclitaxel/β-cyclodextrin nanocomplex

2.6.1. Morphological observation

The microstructure and morphology of the hydrogel formulations were examined using an FEI Quanta 250 FEG scanning electron microscope at 8000.0 magnification. First, the hydrogels were cryopreserved with dry ice for 2 h. Then, freeze-drying was performed using an Alpha 1–2 LD plus instrument over two days to eliminate significant water from the hydrogels. Precision blades were employed to cut the hydrogel samples, which were then affixed to the SEM holder with conductive silver paint. Finally, the samples were coated with carbon using a Leica EM ACE200 low vacuum coater.

2.6.2. Rheological characterization

Rheological analysis was performed using a Thermo Haake Rheometer from the United States. The hydrogels were evenly applied to a 25 mm-wide parallel plate and sealed with silicone oil to prevent solvent evaporation. A thorough frequency scan was conducted over a range of 0.1 to 100 rad/s to assess the storage modulus (G') and loss modulus (G''). The measurements were carried out at a stress amplitude of 0.1 % and a temperature of 25 °C.

2.6.3. Porosity measurement

The overall porosity of the hydrogels was measured using the liquid displacement method, based on a previous study with slight alteration (Yom-Tov et al., 2014). The samples (around 25 mg) were submerged in a displacement liquid (absolute ethanol) with known volume (v_1) for one h. The volume (samples with ethanol) was measured (v_2). Then, the samples were removed, and the volume of the remaining ethanol was measured (v3). The porosity was calculated using the following calculation.

$$\varepsilon = \left(\frac{v1 - v3}{v2 - v3}\right)$$

2.6.4. Swelling dynamics

Hydrogel swelling was measured using the Japanese Industrial Standard K8150 method. As outlined in this protocol, the dried hydrogel was immersed in deionized water for 48 h at room temperature on a roller mixer. After swelling occurred, the hydrogel was filtered through a stainless steel mesh with a mesh size of 30, equivalent to 681 μm. The swelling calculation was performed as follows.

$$Swelling(\%) = \left(\frac{Ws - Wd}{Wd}\right) \times 100$$

In this scenario, Ws denotes the weight of the hydrogel when swollen, and Wd represents its weight in a dry state.

2.6.5. In vitro degradation measurements

The degradation rate of the hydrogels was assessed by monitoring mass loss. To achieve this, the weight of each dried hydrogel disk was

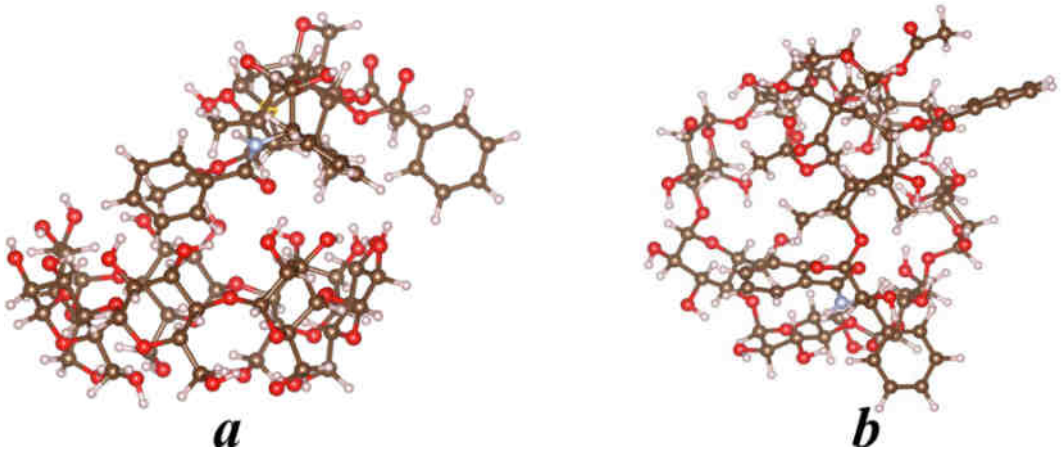

Fig. 2. Optimum configurations obtained PTX adsorption inside β-CD surface by using MC simulation in Material Studio 2017. The first conformation features PTX atoms arranged loosely (a), while the second conformation showcases PTX atoms densely packed together (b).

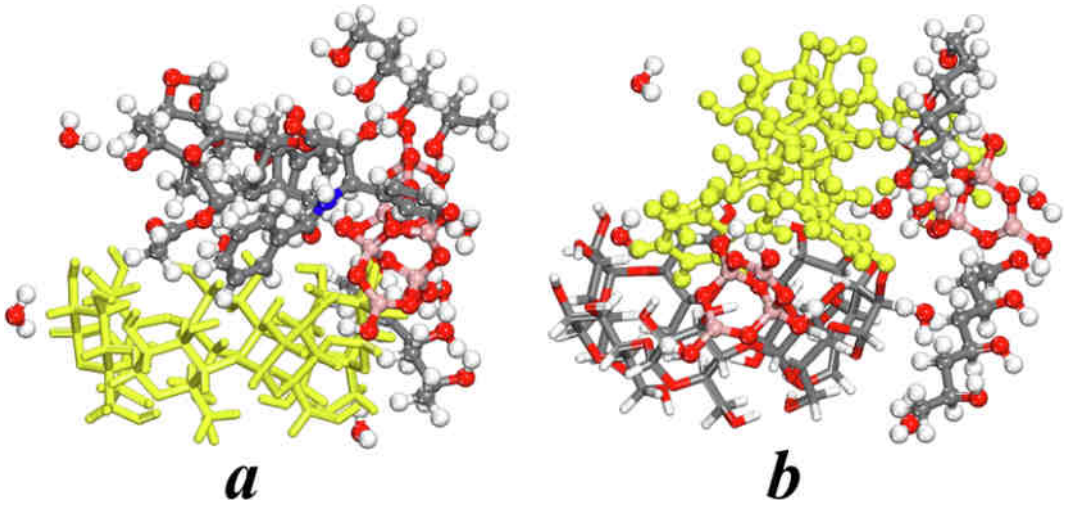

Fig. 3. The equilibrium state of B and PVA adsorption on the PTX/β-CD to form B/PVA/PTX/β-CD by adsorption locator module in Materials Studio 2017 software. It illustrates the interaction of B and PVA with both the tightly packed (a) and the more open conformations of the PTX/β-CD complex (b).

recorded, and uniform-sized samples were immersed in a Falcon tube filled with phosphate-buffered saline (PBS) at 37 °C. Weight loss measurements were taken at predetermined time intervals. Triplicate samples from each group were removed from the solution and dried at various time points. The mass of the samples was then measured to evaluate the extent of degradation using a specific equation.

$$\text{Weight loss}(\%) = \left(\frac{W_0 - W_1}{W_0}\right) \times 100$$

where W_0 represents the initial weight of the hydrogels, and W_1 represent the desiccated weight after removal from the water.

2.6.6. Evaluation of in vitro release

The release of PTX from the sample in vitro was assessed using UV–visible spectroscopy. The βCD/PTX-PVA-borax hydrogel inclusion complexes (1 mL) were incubated in 5 mL of PBS at neutral (pH 7.4) and acidic (pH 3.4) conditions at 37 °C. At regular intervals (0.25, 1.0, 1.5, 2.0, 4.0, 6.0, 8.0, 24.0, 48.0 h), 1 mL of the supernatant was collected, and an equal volume of fresh PBS was added. After centrifugation, the absorbance intensity of the resulting supernatant was measured at a wavelength of approximately 230 nm.

2.6.7. Mechanism of drug release

Four kinetic models—the zero-order kinetic model, the first-order kinetic model, the simplified Higuchi model, and the Korsmeyer-Peppas model—were used to study in vitro release patterns in order to evaluate the mechanism of drug release.

Drug dissolution that is unaffected by drug concentration is linked to the zero order model.

$Q_t - Q_0 + K_0 t$

The concentration-dependent drug release is described by the first order model.

$$\frac{Dc}{dt} - kC$$

The following equation is used by the simplified Higuchi model to explain drug release from matrix and polymeric systems.

$$\frac{Mt}{M\infty} - k\sqrt{t}$$

The following equation is used by the Korsmeyer-Peppas model to describe drug release from matrix and polymeric systems.

$$\frac{Mt}{M\infty} - k't^n$$

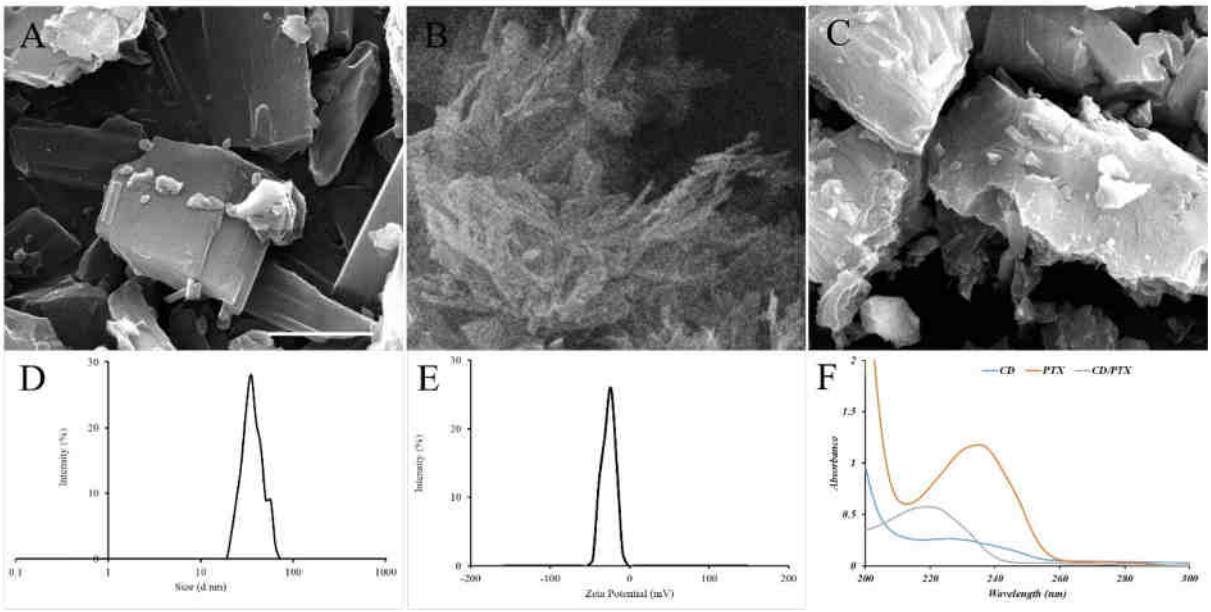

Fig. 4. The characteristics of the complex. (A) SEM image of pure β-CD, (B) SEM image of the pure PTX, (C) SEM image of PTX/β-CD inclusion complex, (D) DLS result of PTX/β-CD inclusion complex, (E) Zeta potential of PTX/β-CD inclusion complex, and (F) UV–Vis spectrum of the components. The pure CD exhibited flat shape and pure PTX exhibited sticklike morphology and PTX/β-CD inclusion complex exhibited the combination morphology. The zeta potential of the PTX/β-CD inclusion complex and we found that the complex has a zeta potential of −26.8 ± 3.1 mV.

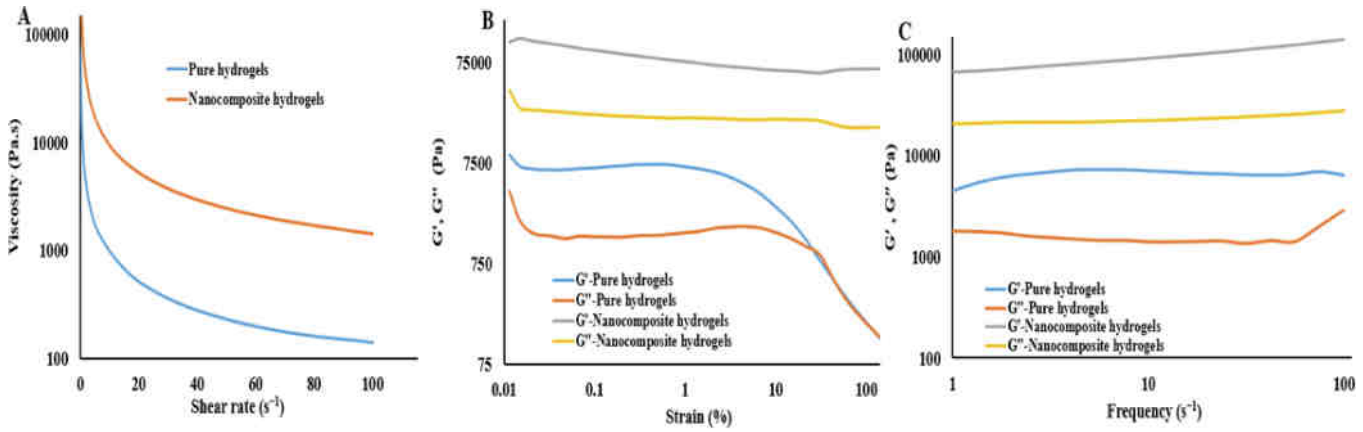

Fig. 5. Rheological evaluation of pure and nanocomposite hydrogels includes: (A) viscosity profiles, (B) strain amplitude sweeps during dynamic oscillatory shear, and (C) frequency response during dynamic oscillatory shear.

2.7. Biological and anticancer evaluations

2.7.1. MTT assay for anticancer efficacy

The MTT assay was employed to evaluate cell activity on the hydrogels quantitatively. Cells (Pan02 cells were obtained from the American Type Culture Collection) were seeded at a density of 1×10^4 cells onto 150 μl of hydrogels in Dulbecco's modified Eagle's medium: nutrient mixture F-12 (DMEM/F12; Gibco, Grand Island, USA). The medium contained 10 % fetal bovine serum (FBS; Gibco, Grand Island, USA), 100 units/ml penicillin (Sigma-Aldrich, USA), and 100 μg/ml streptomycin (Sigma-Aldrich, USA). The cell culture was incubated in a humidified environment at 37 °C with 5 % CO_2. The cell culture medium was collected from the 96-well plate at designated time points (1 and 3 days after cell seeding). Following this, 0.2 ml of MTT solution (0.5 mg/ml) was added to each well and incubated at 37 °C for 3 to 4 h in the dark. After incubation, the MTT solution was removed, and 0.1 ml of DMSO was added to dissolve the purple formazan crystals. The absorbance was measured at approximately 570 nm using a microplate reader (Anthos 2020, Biochrom, Berlin, Germany). Mean values from triplicate wells for each sample were recorded.

2.7.2. Scratch assay and transwell migration/invasion assay for anti-metastatic potential

The study involved conducting a wound-healing test and a scratch assay, using cells plated in coated wells to assess cell migration rates. Initially, the cells were seeded at a density of 1.5×10^4 cells per well. Once the cells reached confluence, a p20 pipette tip was used to create a "wound" by scratching a gap across the cell monolayer. The average initial gap area was measured at 2.2098 mm^2, with a standard deviation of 0.4201 mm^2. Following this, cell migration was observed and recorded at various time intervals. Three replicates were performed for each experimental and control condition. In our experimental setup, we utilized 24-well plates with transwell chambers having an 8 μm pore size manufactured by Corning. The transwell migration tests were performed using these plates. The cells were seeded statically on top of hydrogel to migrate through the hydrogel matrix and were assessed using a

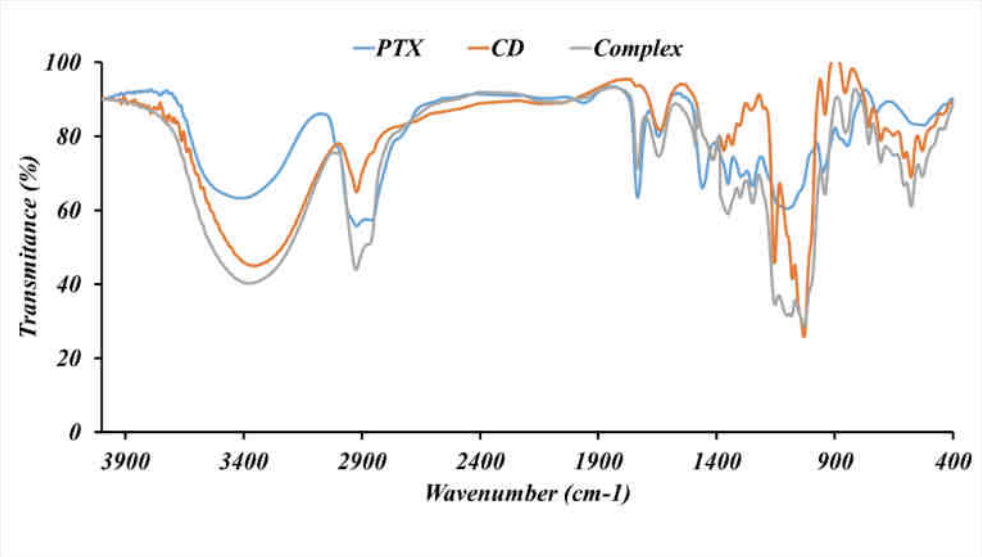

Fig. 6. FTIR spectrum of the synthesized PTX/β-CD inclusion complex. The spectrum exhibited the characteristics peaks of pure PTX and pure β-CD, while the there are some shifts in the peaks in the spectrum of the inclusion complex.

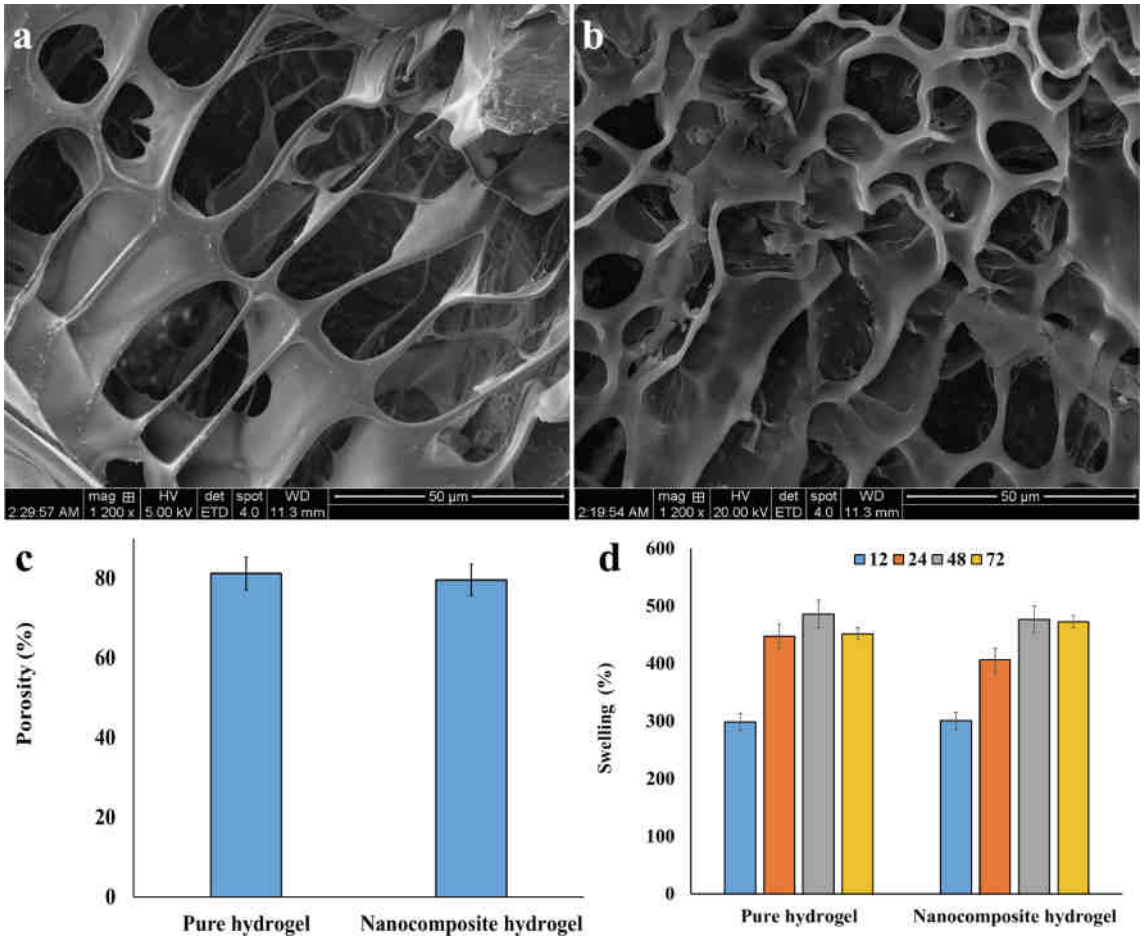

Fig. 7. The characteristics of the fabricated hydrogels. (a) SEM image of pure hydrogel, (b) SEM image of nanocomposite hydrogel, (c) Porosity of the hydrogels, and (d) Selling of the hydrogels. N: 3, Data presented as means ± SD. The hydrogels exhibited a porous structure. The hydrogels have a porosity in the range of 70–90 % with negligible differences. The hydrogels absorb a huge amount of water and swelled more than 400 % of their initial weight.

transwell migration assay. When starting the cell culture, a specified volume of medium without FBS was used to suspend the cells at pre-determined quantities, achieving the desired final cell concentration in the FBS-free medium. The cell suspensions in the FBS-free medium were added to the upper chamber, while the lower chamber beneath the membrane was filled with medium containing 10 % FBS, creating a

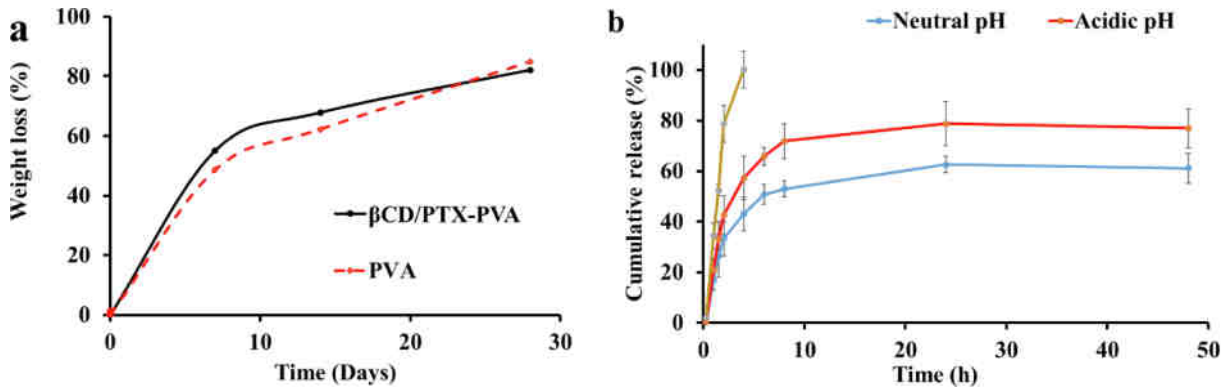

Fig. 8. (a) Weight loss of the fabricated hydrogels and (b) Release of PTX form the hydrogel. N: 3, Data presented as means ± SD. The biodegradation rate of pure hydrogel and β-CD/PTX hydrogel were around 82.1 % and 84.8 %, respectively, during 28 days, indicating acceptable biodegradation profile. The β-CD/PTX inclusion complex loaded hydrogel exhibited a sustained and pH-dependent release, while free PTX-loaded hydrogel exhibited uncontrolled and burst release.

nutritional gradient.

All experimental groups were incubated under appropriate atmospheric conditions at 37 degrees Celsius for 24 h. After incubation, the samples were gently washed three times with PBS. The samples were then fixed using a 4 % paraformaldehyde solution from Service Bio. Next, they were stained with a 0.1 % crystal violet solution, also obtained from Service Bio. Cell behavior was observed using Nikon Ti Inverted Microscopes in brightfield mode. To evaluate cell migration in the different experimental groups, the number of cells in the lower chamber below the membrane was quantified. Five random fields from each sample image were selected, and the average cell count was calculated.

2.7.3. Determining anticancer mechanism

The acridine orange/propidium iodide (AO/PI) double staining was used to investigate the apoptosis of the cells under incubation of the hydrogels. After incubating with the hydrogels, the cells were washed twice with PBS and incubated with 10 μg/ml of AO/PI for 5 min in the dark at 37C. The stained cells were washed three times with PBS and observed under a fluorescence microscope with an excitation wavelength of 488 nm.

2.8. Reactive oxygen species (ROS) assay

The ROS level in the cancer cells was evaluated using the DCFH-DA staining assay. The induced ROS oxides DCFH-DA are converted into highly fluorescent DCF that can be observed under a fluorescence microscope. After incubating with the hydrogels, the cells were washed twice with PBS and incubated with 20 μM of DCFH-DA for 30 min in the dark at 37C. The stained cells were washed three times with PBS and observed under a fluorescence microscope with an excitation wavelength of 488 nm.

2.9. Animal studies

After receiving approval from the Animal Ethics Committee, the animal investigations were carried out on male C57BL/6 mice weighing between 18 and 20 g. The meticulously cared-for animals were examined under stringent criteria in a typical laboratory setting. To create the xenograft pancreatic tumor models, 1×10^7 cells in 100 μL of Hank's solution were injected subcutaneously into the right flank of the mice. Animals were grouped once the tumor volume had reached 100 mm3. The mice were split into three groups at random, each consisting of five mice: β-CD/PTX/PVA (the tumor model with β-CD/PTX/PVA), PVA (the tumor model with pure hydrogel), and Control (the tumor model with saline injection). A 29G needle syringe was used to inject the hydrogel into the tumor locations. Every two days, the body weight was recorded. Half of the mice were euthanized on day 25 following treatment, and the tumors from those mice were gathered. The tumors were weighed and measured for size. For the purpose of survival analysis, the remaining mice (n = 5) were continually observed.

2.10. Statistical analysis

The obtained data were statistically analyzed using SPSS 17.0 (SPSS, Inc., Chicago, IL, USA) by one-way analysis of variance followed by Fisher's least significant difference. The data obtained from at least triplicate experiments and expressed as the mean ± SD. A p-value less than 0.05 was considered to indicate a statistically significant difference.

3. Results and discussion

3.1. Monte Carlo (MC) simulation of PTX loading inside β-CD to form PTX/β-CD

Monte Carlo simulations were conducted to investigate the impact of molecule adsorption on the surface of the adsorbent (Haounati et al., 2023). β-CD was selected for the adsorption studies in this simulation due to its cavity sites. The adsorption of PTX onto β-CD molecules in a 1:1 ratio was performed to generate a composite, utilizing the adsorption locator module in Materials Studio 2017 software. Following the optimization of all compounds, the most stable structure of PTX adsorbed within the β-CD carrier was determined using molecular dynamics (MD) simulations, as illustrated in Fig. 2a and b. The estimated adsorption energy (Eads) of PTX within β-CD to form the PTX/β-CD complex was -1.133×10^{-3} kJ/mol. This negative adsorption energy indicates that the adsorption process is exothermic, reflecting a strong interaction between PTX and the β-CD cavity. Although PTX features hydroxyl groups and oxygen atoms, its overall hydrophobic structure results in it being located within the β-CD (Ganjali Koli et al., 2023). The analysis exhibited that PTX strongly tended to form hydrogen bonds with the neighboring –OH group in the cavity site of β-CD surface (Ganjali Koli et al., 2023).

3.2. Monte Carlo (MC) simulation of B and PVA loading on PTX/β-CD surface to form B/PVA/PTX/β-CD

The most stable adsorption configurations of two molecules of B and PVA on the PTX/β-CD carrier were simulated using the adsorption locator, with the equilibrium configurations illustrating the adsorption system displayed in Fig. 3a and 3b. In the Monte Carlo (MC) method, van der Waals forces and electrostatic interactions were considered based on group-based interactions with a cutoff radius of 12.5 Å. The interaction energy of B and PVA on PTX/β-CD was −319.150 kJ/mol, suggesting

Table 1
Literature findings on the drug delivery systems

Formulation	Type	Benefits, Aims, and OtherNotes	Ref
Albumin-coated PTX-NC (Alb-PTX NCs)	Nanocrystal	High drug loading (90 %) and serum stability Equivalent cytotoxicity. More stability in undiluted serum.Less interaction with serum proteins.	(Park et al., 2017)
Surface modified PTX-NCs with apo-transferrin (Tf) or hyaluronic acid (HA)	Nanocrystal	PTX release was faster. Improve the cellular uptake, permeability, and cell growth inhibition (60 %) against the cancer cells. The effect on the normal cells was inferior. Provide targeted delivery to cancer cells.	(Sohn et al., 2017)
PEGylated PTX NCs	Nanocrystal	superior stability under both storage and physiological conditions. In vivo studies showed significant improvement of the antitumor activity in facing in situ or metastatic tumor	(Zhang et al., 2015)
PEGylated polyelectrolyte multilayer-coated PTX NCs	Nanocrystal	Slowed down the dissolution. Offered colloidal stability in physiologically simulated media. Showed no innate effect on cell viability using HT-29 cells.No hemolytic activity was detected.	(Polomska et al., 2017)
PTX NCs modifiedwith PEG and folic acid(FA) (PTX NCs-PEG-FA)	Nanocrystal	Improved cellular uptake and growth inhibition in cells.An in vivo pharmacokinetic study showed a significant increase in the circulation of PTX.	(Zhao et al., 2021)
urface-modifiedPTX with positively charged poly (allylamine hydrochloride) (PAH)	Nanocrystal	Higher drug release. Stronger interaction with bovine serum albumin.Greater cellular internalization, uptake, and cytotoxicity.	(Choi and Park, 2016)
Pluronic-grafted chitosan as a stabilizer for PTX NC(Pl-g-CH PTX NCs)	Nanocrystal	Improving intra-cellular accumulation. Improving the absorption by the transcellular and paracellular routes. Showed a P-gp inhibitory property.	(Sharma et al., 2015)
Transferrin (TF)-modified PTX NCs	Nanocrystal	Showed an enhancement of cellular monolayer penetration. Had superior suppression in MCF-7 cell growth.Showed an enhancement of intestinal absorption.	(Han et al., 2020)
PTX NC-loaded PECT hydrogels	Hydrogel	High loading capacity of the drug. In vitro release was more effective and homogeneous.	(Lin et al., 2016)
PTX NC with F127 hydrogel	Hydrogel	PTX NCs gel offered optimum properties with high drug loading combined with moderate drug release and erosion profiles. Superior anti-tumor efficacy in 4 T1 tumor-bearing BALB/c mice.	(Lin et al., 2015)
In situ cross-linkable hydrogel depot containing PTX NCs	Hydrogel	Superior killing efficiency and more toxicity in SKOV3 cell line. The in vivo study indicated improved dissolution, cellular uptake, and lower maximum tolerated dose.It also showed that a single IP dose was sufficient in extending the survival of tumor-bearing mice.	(Sun et al., 2016)
PTX-NCs combined with niclosamide (NLM) NLM-NCs co-loaded PLGA-PEG-PLGA thermosensitive hydrogel (PN-NCs-Ts)	Hydrogel	Sustained and significantly delayed drug release both in vitro and in vivo. The combination with NLM improved PTX cellular uptake, apoptosis, and provided inhibition of cell migration.	(Zhao et al., 2021)

that the adsorption was energetically favorable and interacted strongly to form B/PVA/PTX/β-CD (Haghbin et al., 2023). Conversely, the adsorption of the B and PVA molecules on the PTX/β-CD surface was spontaneous.

3.3. The release PTX from B/PVA/PA/β-CD composite

The behavior and release mechanism of PTX were studied under neutral (pH = 7.4) and acidic conditions (pH = 3.4). The release energy of PTX from the B/PVA/PTX/β-CD composite was assessed using the DFT-D method via the DMol^3 module. The binding energy ($E_{binding} = E_{interaction}$) for B/PVA/PTX/β-CD was found to be −60.977 at pH 3.4 and −69.312 at pH 7.4. DFT-D simulations indicated that the binding energy of the PTX molecule within the composite was lower in the acidic solution compared to the neutral one. Consequently, PTX was more readily released from B/PVA/PTX/β-CD at the lower pH (3.4) due to the cationic form of the hydroxyl groups (Ganjali Koli et al., 2023).

3.4. Characteristics of the structures

We applied SEM imaging technique to observe the morphology of pure β-CD (Fig. 4A), pure PTX (Fig. 4B), and the PTX/β-CD inclusion complex (Fig. 4C). Moreover, we applied the SEM imaging to evaluate the morphological change of the components after forming the complex. It can be seen that the pure β-CDs have plate-like morphology with smooth surface, while PTX has a sticklike morphology. On the other hand, the synthesized PTX/β-CD inclusion complex exhibited different morphology, indicating the formation of the PTX/β-CD inclusion complex. The observed morphological change after the formation of the inclusion complex agrees with previous studies. Choi et al. (Choi et al., 2014) synthesized mucoadhesive and thermosensitive sol–gel composites loaded with PTX/dimethyl-β-CD for buccal delivery and reported the same morphological observation.

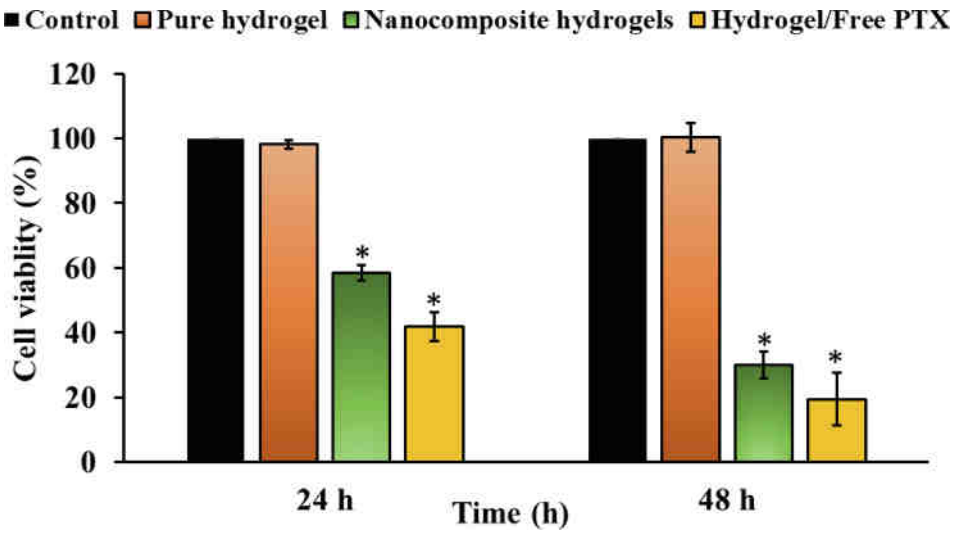

Fig. 9. Results of cell viability under treatment with hydrogels at 24 and 48 h, measured by the MTT assay. Control (the cells treated with PBS) N: 3, Data presented as means ± SD. ANOVA, (*) $p < 0.05$.

Additionally, UV–Vis spectroscopy was employed to evaluate the inclusion complex formation between PTX and CD. The results (Fig. 4F) revealed that the combination exhibited a redshift in its maximum absorbance compared to pure PTX, indicating the presence of the guest molecule. The observed hypsochromic shift in the absorption maxima of PTX suggests that it has been successfully incorporated into the cavity of β-cyclodextrin.

The DLS technique showed that the complexes have a hydrodynamic diameter of around 110 nm (Fig. 4D). We evaluated the zeta potential of the PTX/β-CD inclusion complex and we found that the complex has a zeta potential of −26.8 ± 3.1 mV (Fig. 4E). A negative charge at the surface suggests that the amphiphilic β-CDs' molecular alignment is such that the un-substituted –OH groups point in the direction of the aqueous environment, perhaps resulting in surface hydrophilicity (Rachmawati et al., 2013). The high zeta potential confirmed the idea that the inclusion complex solution is stable because its particles have enough interparticle repulsion to keep them from aggregating. A relatively stable system is reached when a solution's zeta potential is high because the repulsive force outweighs the attraction.

Hydrogels are polymeric networks that can absorb and retain water, and their rheological properties are crucial for understanding their behavior under stress and flow. A series of mechanical parameters can characterize a hydrogel's stiffness or elasticity. The stiffness or elasticity of a hydrogel can be described through various mechanical parameters. A common method used for quantitatively assessing the resistance to deformation, as well as the flow resistance (viscosity) of polymer solutions, is rheological analysis or viscometry.

Initially, the measured rheological parameters were used to evaluate the shear thinning behavior of the hydrogels, with the findings illustrated in Fig. 5A. The graph indicates that as the shear rate rises, viscosity diminishes. Both types of hydrogels—pure and nanocomposite—exhibit shear-thinning behavior and are classified as non-Newtonian fluids. The i incorporating PTX/β-CD into the hydrogel enhanced gelation, resulting in a higher viscosity for the nanocomposite hydrogel than the pure hydrogel. To evaluate the storage (G′) and loss (G″) moduli, oscillatory rheological tests were performed on both the pure and nanocomposite hydrogels. The oscillatory strain sweeps results (Fig. 5B) demonstrate that both hydrogels exhibit elastic solid behavior across a broad range of strains, as indicated by the storage modulus G′ being greater than the loss modulus G″. Fig. 5C illustrates the results of frequency sweep tests in the linear viscoelastic (LVE) region of the hydrogels, as referenced in Fig. 5B. The pure hydrogels exhibit limited mechanical strength, while the nanocomposite hydrogels consistently show a storage modulus (G′) that exceeds the loss modulus (G″) across all tested frequencies. This highlights their elastic dominance. The addition of β-CD and the resulting intramolecular interactions significantly bolster the mechanical properties of the nanocomposite hydrogels. Various interactions, such as Van der Waals forces, electrostatic attractions, and hydrogen bonding, likely contribute to this increased strength. These results suggest that the hydrogels are well-suited for applications in dermatology.

The formation of a complex between a guest molecule and β-CD can be confirmed by evidence gathered through infrared (IR) spectroscopy. This complexation typically leads to changes in the characteristic absorption peaks of the guest molecule. In the pure PTX spectrum, the peak at approximately 1460 cm^{-1}, attributed to the benzene ring, is obscured in the PTX/β-CD inclusion complex, demonstrating the formation of the inclusion complex (Fig. 6). The FTIR spectrum of β-CD exhibited a characteristic peak at 2926 cm^{-1} (for the C–H stretching vibration), 3,300–3,400 cm^{-1} (for the asymmetric/symmetric–OH stretching vibration due to the many intermolecular hydrogen bonds), and 1023 cm^{-1} (for the symmetric C–O–C stretching vibration). As expected, the indicated peaks of the β-CD and the characteristics peaks of PTX (the absorption bands in the range of 1750–1600, 1300–1180, and 770–630 cm^{-1}) can be found in the inclusion complex, with negligible shifts. Additionally, the broadening of the –OH band around 3400 cm^{-1} in the PTX/β-CD inclusion complex signifies the presence of hydrogen bonding between PTX and β-CD, further supporting the formation of the complex (Ye et al., 2015). These data suggest that the PTX/β-CD inclusion complexes were successfully formed.

The hydrogels were thoroughly analyzed using suitable methods to reveal their physical and chemical characteristics. SEM imaging was utilized to investigate the internal structure of the hydrogels, showing a porous nature for both the pure and nanocomposite hydrogels, as depicted in Fig. 7a and 7b. We found that the incorporating the PTX/β-CD inclusion complex did not affect the internal morphology of the hydrogel. We assessed the porosity of the hydrogels using the liquid displacement method and found that the porosity ranged from 75 % to 85 % (Fig. 7c). Additionally, swelling measurements of the hydrogels (Fig. 7d) indicated that they could absorb water up to approximately 500 % of their dry weight. Huabo et al (Huang et al., 2016), synthesized polyaniline/PVA conducting hydrogel and reported the porous and interconnected microstructure. In a separate investigation, Ehab Al-Emam and colleagues documented the presence of highly interconnected pores within the 3D framework of PVA-Borax hydrogel. (Al-Emam et al., 2020). The prediction of drug molecule release from a

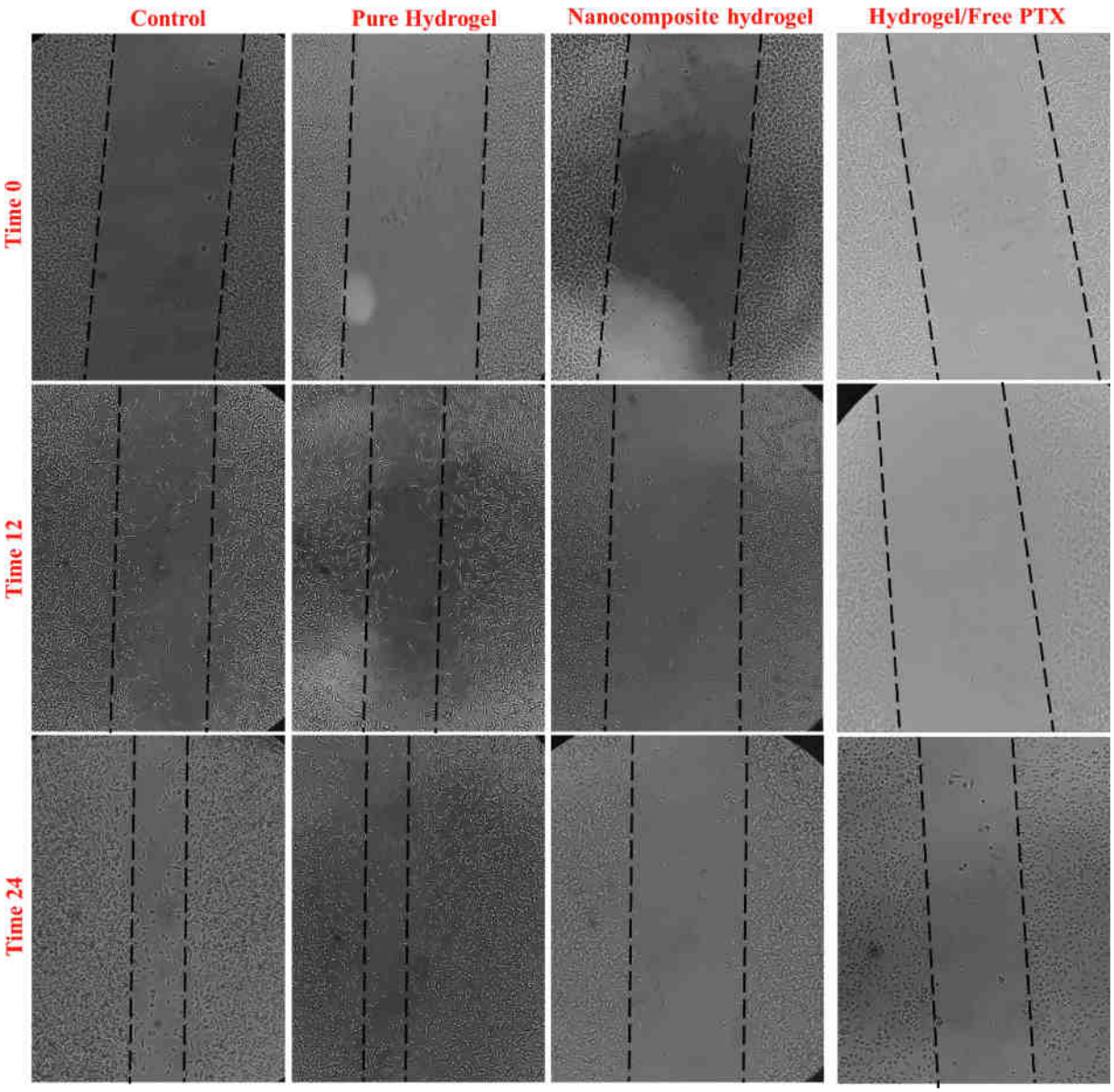

Fig. 10. Scratch/wound healing results of the cells.

hydrogel matrix typically depends on the evaluation of several parameters, such as swelling behavior, viscosity, pH sensitivity, biodegradability, and the degree of cross-linking. While these features give an overview of the hydrogel system, they do not fully characterize its individual components. Properties like porosity and dielectricity offer unique advantages over other characteristics, as they provide important insights into pore size determination and the analysis of admittance and dielectric relaxation, respectively.

The degradation of the hydrogels in PBS solution (Fig. 8a) was observed over a 28-day period. The results indicated that the hydrogels lost approximately 80 % of their initial weight during this time, demonstrating that the fabricated hydrogels are biodegradable. Biodegradable scaffolds play a crucial role in tissue engineering, serving as temporary structures that replicate the mechanical and biological properties of the original extracellular matrix (ECM). These scaffolds facilitate cell adhesion, invasion, proliferation, and differentiation, ultimately aiding in the regeneration of functional tissue or the natural ECM (Domb and Khan, 2020).

We evaluated the release profile of PTX from the fabricated hydrogel under different conditions (neutral and acidic pH), and the results are presented in Fig. 8b. The results showed that free PTX was released from the hydrogel very fast during the first five hours. This observation showed that free drug (un-complexed) drug is not suitable for sustained drug delivery applications. On the other hand, it can be seen that the complexation resulted in sustained drug delivery. The findings indicated that, in both conditions, the produced hydrogel initially exhibited a burst effect in drug release, followed by a sustained release. The obtained results are well-matched with the simulation studies, indicating that hydrogen interaction between β-CD with the drug and B/PVA/PA was decreased by creating acidic conditions. As a result, the release of drug was increased. Under acidic conditions, the hydrogen bonding interactions between β-CD and the drug, as well as between β-CD and the B/PVA/PA matrix, were found to decrease. This can be attributed to the protonation of functional groups (such as hydroxyl or amine groups) present on β-CD and the polymeric matrix (B/PVA/PA) in the acidic environment. Protonation leads to a reduction in the electron density of the donor sites involved in hydrogen bonding, thereby weakening the interactions between the β-CD cavity and the drug molecules or the polymer matrix. As a result, the stability of the drug-β-CD complex is reduced, which may facilitate the release of the drug from the carrier

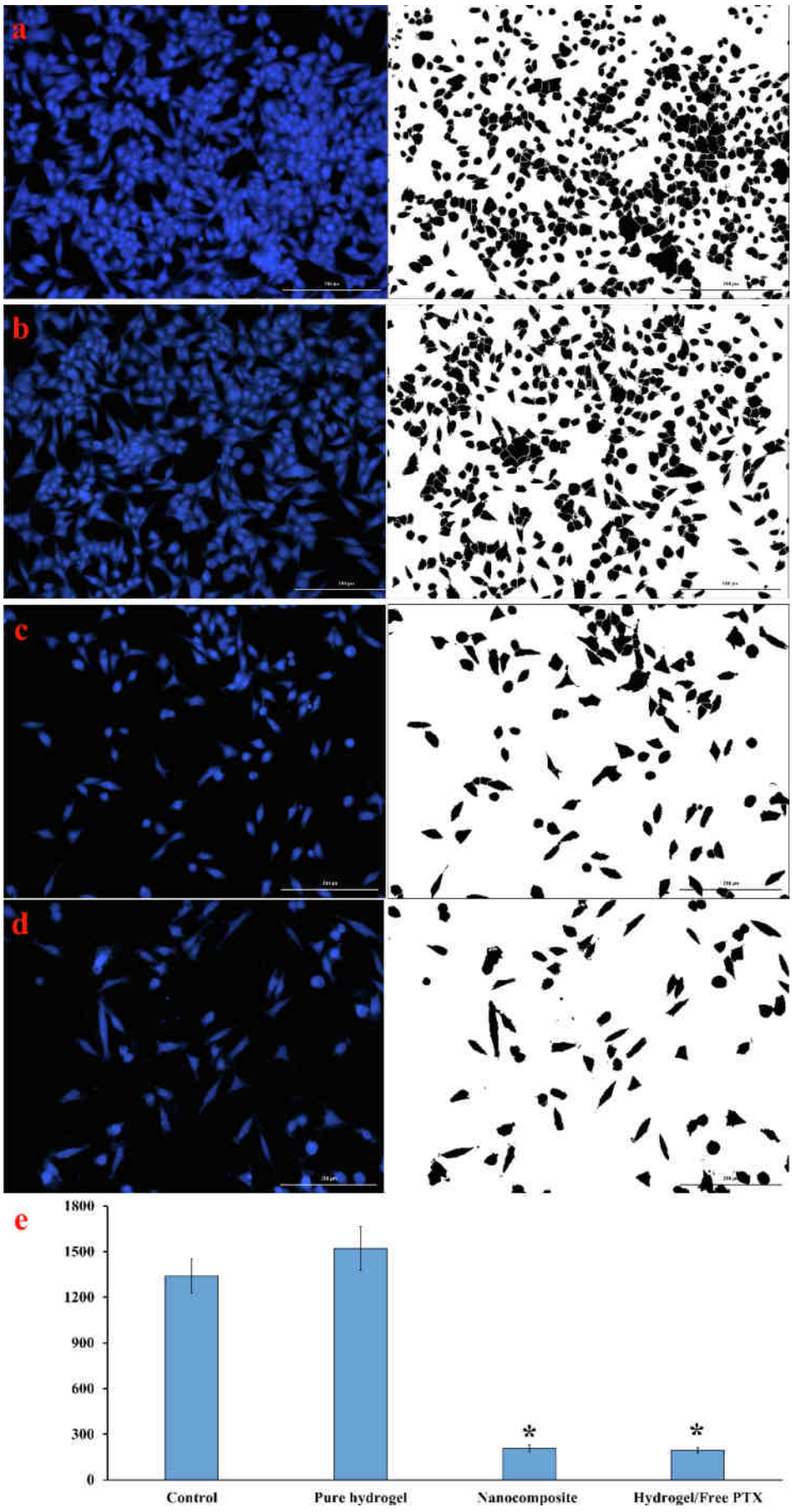

(caption on next page)

Fig. 11. Invasion assay results of the cells, evaluated via the Transwell invasion assay. (a) Negative control (cancer cells without treatment), (b) Cancer cells treated with pure hydrogel, (c) Cancer cells treated with nanocomposite hydrogel (d) Cancer cells treated with hydrogel/Free PTX, and (e) Comparative analysis of the negative control sample (untreated cancer cells), cancer cells treated with pure hydrogel, and cancer cells treated with the nanocomposite formulation. Control (the cells treated with PBS). N: 3, Data presented as means ± SD, one-way ANOVA, (*) $p < 0.05$.

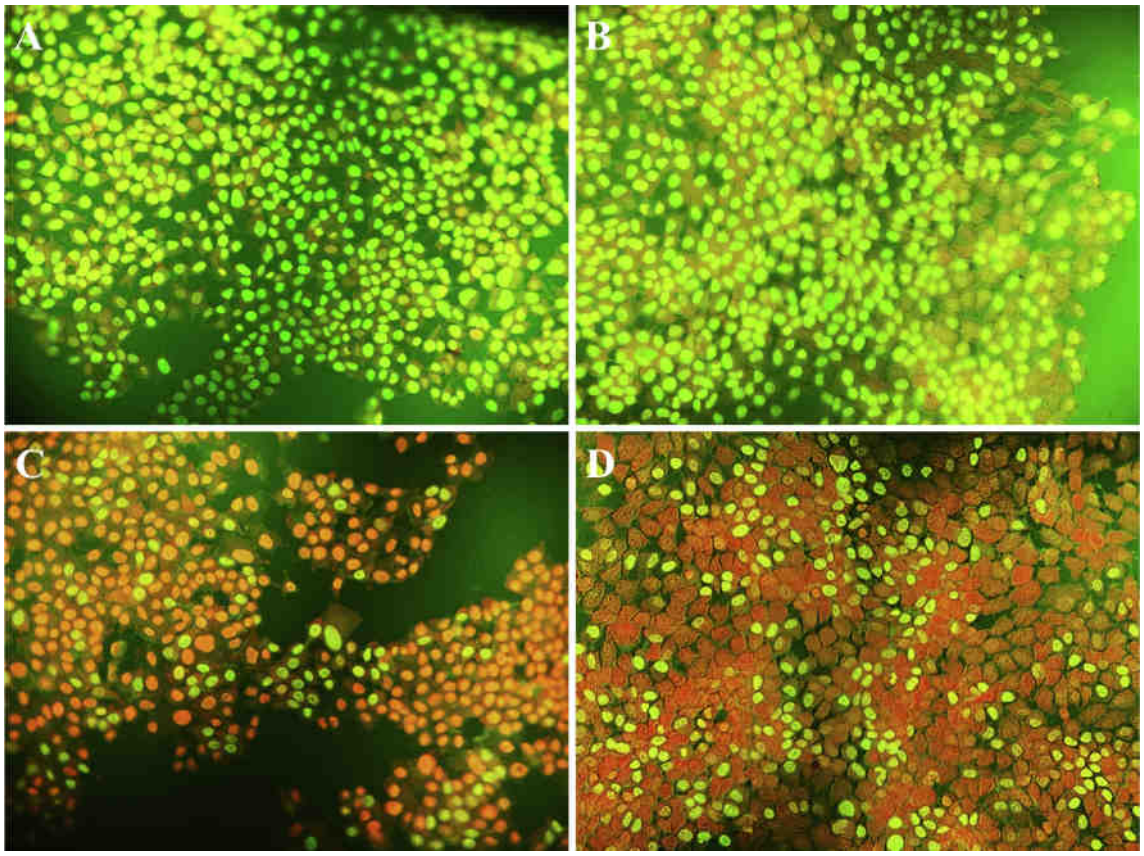

Fig. 12. Acridine orange/propidium iodide double staining of the cells. (A) Control group (the cells treated with PBS)), (B) Cancer cells treated with pure hydrogel, (C) Cancer cells treated with PVA/PTX/β-CD-loaded hydrogel, and (D) Cancer cells treated with hydrogel/Free PTX. N: 3.

system under acidic conditions. Moreover, it has been shown that the pH-triggered release from PVA/Borax hydrogel can be due to the weakening of the boronic acid-hydroxyl interactions in acidic pH and the instability of hydrogel. These changes in the interaction dynamics are significant for drug delivery systems where pH-sensitive release profiles are desired, particularly in environments like the stomach, which is naturally acidic. The Korsmeyer-Peppas model showed the strongest correlation with drug release, indicating that the aggregate drug release from multi-layered gold nanoparticles could be described as a polymeric system undergoing degradation.

Hydrogel delivery methods have proven effective in harnessing the therapeutic benefits of drug delivery and are now being utilized in clinical settings. Hydrogels can precisely regulate therapeutic agents' spatial and temporal release, accommodating a wide array of substances, including small-molecule drugs, macromolecular pharmaceuticals, and cells. Their versatility makes hydrogels an excellent tool for managing drug delivery, thanks to their flexible nature, customizable degradation rates, and ability to protect sensitive medications from degradation. This enables various interactions between the encapsulated drugs and the hydrogels, allowing for effective control over drug release (Li and Mooney, 2016). Different drug delivery systems have been evaluated for PTX drug delivery. Table 1 summarizes different drug delivery systems.

The effectiveness of the hydrogels developed for cancer treatment was evaluated using the MTT assay, with the results shown in Fig. 9. Clearly, the plain hydrogel had no cytotoxic effects, while the hydrogel containing the PTX/β-CD inclusion complex exhibited a significant toxic effect ($P < 0.05$). Moreover, the hydrogel loaded with free PTX exhibited the highest toxicity, and the observations are consistent with the drug release findings. Chen et al. (Chen et al., 2016) reported that the administration of PTX into oligochitosan- carboxymethyl-β-cyclodextrin induced potent antiproliferative effect on U-87 MG cells. Gong et al. (Gong et al., 2018) prepared a PTX formulation based on functionalized selenium nanoparticles and applied it against breast cancer. hey noticed a marked anti-cancer impact on MCF-7 cells and suggested that the toxicity stemmed from triggering apoptosis through the activation of ROS-mediated p53 and AKT signaling pathways.

The migration and invasion potential of cells treated with hydrogels were assessed using the scratch/wound healing in vitro and Transwell invasion assay. The results (Fig. 10) indicated that treatment with the nanocomposite inhibited the cells' migration potential, while the cells in the control and pure hydrogel groups exhibited potent migration rate. Moreover, free PTXloaded hydrogel significantly reduced the migration potential of the cells.

Cell migration is a critical process in morphogenesis, inflammation, and cancer metastasis. The wound healing assay is a cost-effective and easily replicable method for studying the migration of cancer cells in a laboratory environment. This phenomenon stems from the ability of cells grown in a monolayer to move and reconnect with adjacent cells after an artificial wound is created. The assay involves forming a wound

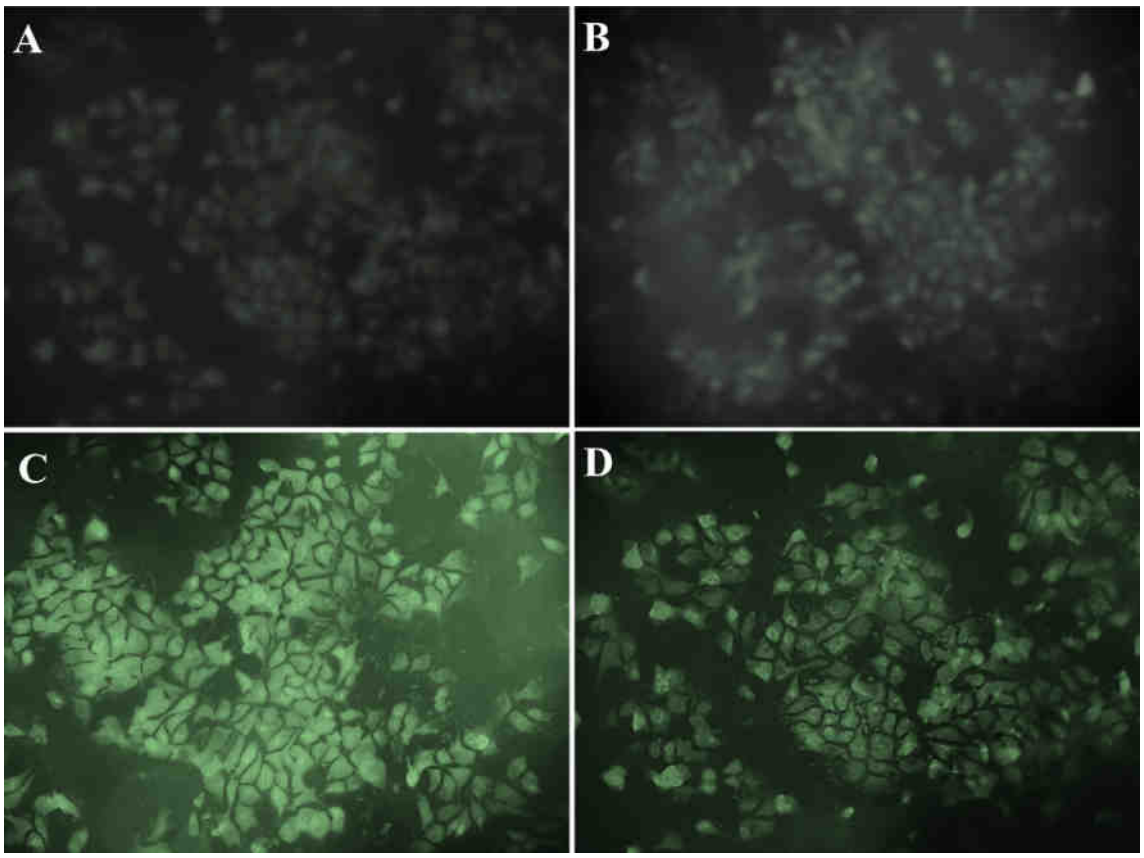

Fig. 13. Intracellular ROS levels evaluation by DCFH-DA. (A) Control group (the cells treated with PBS)), (B) Cancer cells treated with pure hydrogel, (C) Cancer cells treated with PVA/PTX/β-CD-loaded hydrogel, and (D) Cancer cells treated with Free PTX-loaded hydrogel. N: 3.

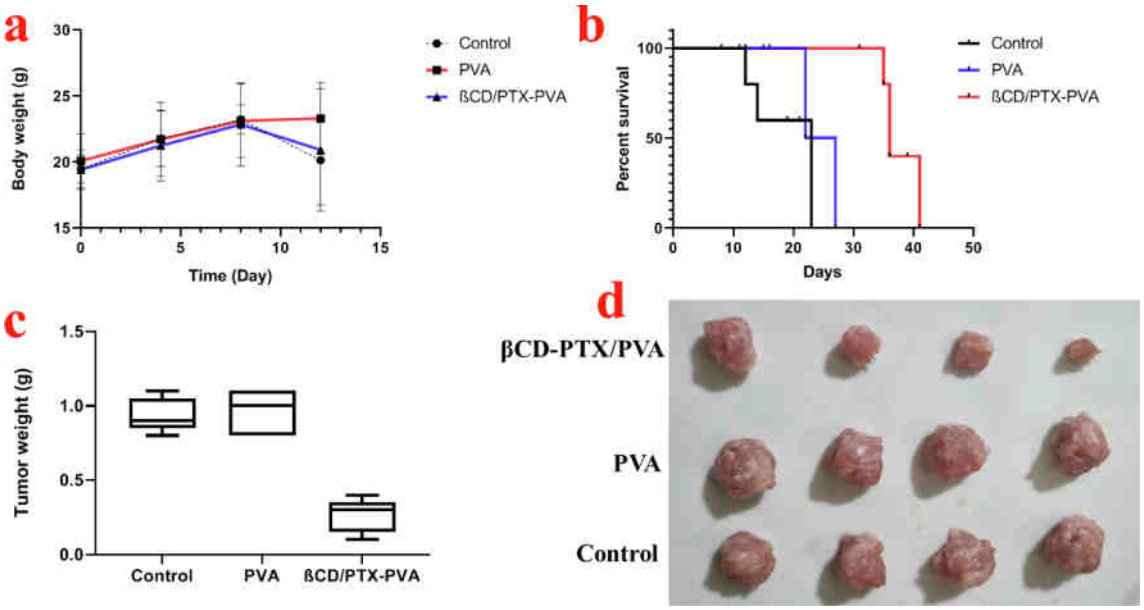

Fig. 14. The anti-tumor efficiency of different groups in vivo. (a) Body weight changes curves of the mice during treatments, (b) Survival curves of mice in different groups, (c) Tumor weight of excised tumors, and (d) The photograph of excised tumors on day 12 post-treatment.

in a single layer of cells, capturing images as the wound heals, and comparing the area covered by migrating cells at both the beginning and end of the experiment. A wound healing assay, also known as a scratch assay, measures the movement of cells across a gap created by scratching in a lab environment. This method can be used to assess cell proliferation and migration, particularly in wound healing and cancer research studies. Tumor cell migration is critical in cancer metastasis, especially during the invasion phase.

The results of the transwell invasion assay (Fig. 11) demonstrated that untreated cells could invade through the well's pores, indicating

their invasive nature. In contrast, the treated cells did not pass through the well, suggesting a suppression of the invasion potential of the cancerous cells. Control (the cells treated with PBS). N: 3. Both the PTX-loaded hydrogels (free PTX-loaded hydrogel and PTX/β-CD inclusion complex) suppressed the cancer cells' invasion potential, indicating the formulations' anti-metastatic.

Using the AO/PI staining, the apoptosis of the cells was evaluated, and the results are presented in Fig. 12. The results showed that there are no apoptosis cells in the control group, and the cells are viable (green), while the cells incubated with PVA/PTX/β-CD-loaded hydrogel and free PTX-loaded hydrogel experiencing early apoptosis (bright orange) and late apoptosis (reddish-orange color). These observations revealed that the PTX-based formulation induced apoptosis.

The ROS level in the cells was evaluated using the DCFH-DA staining as the subsequent and possible mechanism of the cell's lethality. The results (Fig. 13) showed that there is no significant green fluorescent of DCF (the oxidized form of DCFH-DA staining) in the control and pure hydrogel-treated groups (Fig. 13A and B), indicating the normal level of intracellular ROS. On the other hand, the treatment using PVA/PTX/β-CD-loaded hydrogel and free PTX-loaded hydrogel enhanced the production of intracellular ROS.

The precise amount of ROS can vary depending on the cancer stage and the particular cellular context, with a delicate balance between the pro-tumorigenic and cytotoxic effects of ROS within the tumor microenvironment. Intracellular ROS levels are generally thought to be elevated compared to normal cells in PDAC, and they play a significant role in tumor progression by promoting cell growth, invasion, and metastasis, as well as contributing to resistance to therapy. Increased mitochondrial respiration and improved ROS production via the electron transport chain can result from mutations in important genes like KRAS, which are commonly detected in PDAC. Angiogenesis, cell proliferation, survival, and the epithelial-to-mesenchymal transition (EMT) can all be enhanced by moderate amounts of ROS, which can also activate signaling pathways including MAPK and PI3K/Akt. Oxidative stress brought on by high ROS levels can damage DNA and cause genomic instability, both of which can accelerate the growth of tumors and make them resistant to treatment.

3.5. Anti-tumor experiments in vivo

Building on the promising anti-tumor effects of PTX/β-CD-loaded hydrogel in vitro, we used precise intratumoral injection to further examine its effectiveness against tumors in xenograft mouse models. The healing outcomes of the treatment was evaluated via measuring tumor weight, and survival rate of the animals (Fig. 14). We found that the treatment using PTX/β-CD-loaded hydrogel significantly suppressed the growth of tumor and extended the survival rate. On the other hand, the control (the animals bearing tumor treated with normal saline) and pure PVA hydrogel (the animals bearing tumor treated with pure PVA) did not inhibited the growth of the tumor.

4. Conclusions

Although various drugs have been developed for pancreatic ductal adenocarcinoma, their use often results in numerous undesirable side effects, toxicity concerns, and multidrug resistance (MDR). Furthermore, the outlook for patients with pancreatic ductal adenocarcinoma remains poor even after surgery and chemoradiation. Localized delivery of anticancer agents presents several advantages over systemic administration, including (a) targeted drug delivery to the affected site, (b) enhanced drug stability within the delivery system until release, (c) the ability to use lower doses compared to conventional systemic methods, and (d) a significant reduction in side effects and systemic toxicity. In this study, we aimed to develop an effective local drug delivery system for Paclitaxel targeting pancreatic ductal adenocarcinoma. Paclitaxel's solubility and biological activity were enhanced by complexing it with β-cyclodextrin. The inclusion complex was confirmed using FTIR and XRD analyses. The synthesized Paclitaxel/β-cyclodextrin nanocomplex was then incorporated into an injectable hydrogel. We evaluated the physicochemical and structural properties of the resulting injectable hydrogel nanocomposite using SEM, FTIR, XRD, and rheological techniques. The anticancer efficacy of the injectable hydrogel nanocomposite was assessed through MTT assays and invasion and migration assays to determine its anti-metastatic potential. Despite the significant strength of the current study, it has some limitations, such as a lack of proper molecular studies (Real-Time Quantitative Reverse Transcription PCR, Western blotting, and immunohistochemical analysis) to reveal the underlying healing mechanisms. The indicated techniques can be used in future studies. Our findings indicate that this injectable hydrogel nanocomposite can effectively address the limitations associated with systemic delivery of Paclitaxel, presenting a promising advanced therapy for pancreatic ductal adenocarcinoma.

Ethics declarations

Research ethics: The research experiments outlined in this article were approved by the Laboratory Animal Welfare and Ethics Committee at Shanxi Hospital.

Ethical approval: Not applicable.

Consent to participate: Not applicable.

Consent to publish: All authors have read and approved this manuscript.

Data availability statement: All the characterizations, analysis, testing's related work and testing's have solely been responsible by Zhou Xu, and Ninggang Zhang. Additionally, the raw data can be obtained on request from the corresponding authors, Zhou Xu, and Ninggang Zhang.

Author Contributions: Conceptualization, Xiuxiu Li, Weiyu Ma, Zhou Xu, Ninggang Zhang; methodology, Xiuxiu Li, Weiyu Ma, Zhou Xu, Ninggang Zhang; formal analysis, Xiuxiu Li, Weiyu Ma, Zhou Xu, Ninggang Zhang; investigation, Xiuxiu Li, Weiyu Ma, Zhou Xu, Ninggang Zhang; writing—original draft preparation, Xiuxiu Li, Weiyu Ma, Zhou Xu, Ninggang Zhang; writing—review and editing, Shubham Sharma, Ramachandran T, Karthikeyan A, Dhirendra Nath Thatoi, AI Ismail; supervision, Ramachandran T, Karthikeyan A, Dhirendra Nath Thatoi, AI Ismail; project administration, Ramachandran T, Karthikeyan A, Dhirendra Nath Thatoi, AI Ismail; funding acquisition, Ramachandran T, Karthikeyan A, Dhirendra Nath Thatoi, AI Ismail. All authors have read and agreed to the published version of the manuscript.

CRediT authorship contribution statement

Xiuxiu Li: Conceptualization. **Weiyu Ma:** Conceptualization. **Zhou Xu:** Conceptualization. **Ninggang Zhang:** Conceptualization. **Shubham Sharma:** Writing – review & editing, Writing – original draft, Supervision, Project administration, Methodology, Investigation, Funding acquisition, Formal analysis, Conceptualization. **T. Ramachandran:** Writing – review & editing. **A. Karthikeyan:** Conceptualization. **Dhirendra Nath Thatoi:** Writing – review & editing. **AI Ismail:** Writing – review & editing.

Declaration of competing interest

The authors declare that they have no known competing financial interests or personal relationships that could have appeared to influence the work reported in this paper.

Acknowledgment

This research work was funded by Umm-Alqura University, Saudi Arabia under grant number: 25UQU4240002GSSR03.

Data availability

No data was used for the research described in the article.

References

Chandana, S., Babiker, H.M., Mahadevan, D., 2019. Therapeutic trends in pancreatic ductal adenocarcinoma (PDAC). *Expert Opinion on Investigational Drugs* 28 (2), 161–177.

Kenner, B., Chari, S.T., Kelsen, D., Klimstra, D.S., Pandol, S.J., Rosenthal, M., Rustgi, A. K., Taylor, J.A., Yala, A., Abul-Husn, N., 2021. Artificial intelligence and early detection of pancreatic cancer: 2020 summative review. *Pancreas* 50 (3), 251–279.

Truong, L.-H., Pauklin, S., 2021. Pancreatic cancer microenvironment and cellular composition: current understandings and therapeutic approaches. *Cancers* 13 (19), 5028.

Ho, W.J., Jaffee, E.M., Zheng, L., 2020. The tumour microenvironment in pancreatic cancer—clinical challenges and opportunities. *Nat. Rev. Clin. Oncol.* 17 (9), 527–540.

Liu, H., Shi, Y., Qian, F., 2021. Opportunities and delusions regarding drug delivery targeting pancreatic cancer-associated fibroblasts. Adv. Drug Del. Rev. 172, 37-51; (b) Chiaravalli, M., Reni, M., O'Reilly, E.M., Pancreatic ductal adenocarcinoma: State-of-the-art 2017 and new therapeutic strategies. Can. Treat. Rev. 60, 32–43.

Ferrara, B., Pignatelli, C., Cossutta, M., Citro, A., Courty, J., Piemonti, L., 2021. The extracellular matrix in pancreatic cancer: description of a complex network and promising therapeutic options. Cancers 13(17), 4442; (b) Vitorakis, N., Gargalionis, A.N., Papavassiliou, K.A., Adamopoulos, C., Papavassiliou, A.G., 2024. Precision Targeting Strategies in Pancreatic Cancer: The Role of Tumor Microenvironment. Cancers 16(16), 2876.

Chintamaneni, P.K., Pindiprolu, S.K.S., Swain, S.S., Karri, V.V.S.R., Nesamony, J., Chelliah, S., Bhaskaran, M., 2024. Conquering chemoresistance in pancreatic cancer: Exploring novel drug therapies and delivery approaches amidst desmoplasia and hypoxia. *Cancer Lett.* 216782.

Springfeld, C., Ferrone, C.R., Katz, M.H., Philip, P.A., Hong, T.S., Hackert, T., Büchler, M. W., Neoptolemos, J., 2023. Neoadjuvant therapy for pancreatic cancer. *Nat. Rev. Clin. Oncol.* 20 (5), 318–337.

Seufferlein, T., Ettrich, T.J., 2019. Treatment of pancreatic cancer—neoadjuvant treatment in resectable pancreatic cancer (PDAC). *Translational Gastroenterol. Hepatol.* 4.

Bernabeu, E., Cagel, M., Lagomarsino, E., Moretton, M., Chiappetta, D.A., 2017. Paclitaxel: What has been done and the challenges remain ahead. Int. J. Pharmaceut. 526(1-2) (**2017**) 474-495; (b) Singh, S., Dash, A.K., 2009, Paclitaxel in cancer treatment: perspectives and prospects of its delivery challenges. Crit. Rev.™ Therapeut. Drug Carrier Syst. *26* (4).

Wang, F., Porter, M., Konstantopoulos, A., Zhang, P., Cui, H., 2017. Preclinical development of drug delivery systems for paclitaxel-based cancer chemotherapy. *J. Control. Release* 267, 100–118.

Bouquet, W., Ceelen, W., Fritzinger, B., Pattyn, P., Peeters, M., Remon, J.P., Vervaet, C., 2007. Paclitaxel/β-cyclodextrin complexes for hyperthermic peritoneal perfusion–Formulation and stability. Eur. J. Pharmaceut. Biopharmaceut. 66(3), 391-397; (b) Bouquet, W., Boterberg, T., Ceelen, W., Pattyn, P., Peeters, M., Bracke, M., Remon, J.P., Vervaet, C., 2009. In vitro cytotoxicity of paclitaxel/β-cyclodextrin complexes for HIPEC. Int. J. Pharm., 367(1-2), 148–154.

Escobar, K., Carrera, I., Naveas, N., Pulido, R., Manso, M., Guarnieri, J.P.d.O., Lancellotti, M., Cotta, M.A., Corrales-Ureña, Y.R., Rischka, K., 2023. Functionalization of breast implants by cyclodextrin in-situ polymerization: a local drug delivery system for augmentation mammaplasty. *Front. Bioeng. Biotechnol.* 11, 1254299.

Sahu, K.M., Patra, S., Swain, S.K., 2023. Host-guest drug delivery by β-cyclodextrin assisted polysaccharide vehicles: a review. *Int. J. Biol. Macromol.* 240, 124338.

Zhao, J., Wang, L., Zhang, H., Liao, B., Li, Y., **2022.** Progress of research in in situ smart hydrogels for local antitumor therapy: a review. Pharmaceutics 14 (10), 2028; (b) Fakhari, A., Subramony, J.A., 2015. Engineered in-situ depot-forming hydrogels for intratumoral drug delivery. J. Controlled Release, 220, 465–475.

Rizzo, F., Kehr, N.S., 2021. Recent advances in injectable hydrogels for controlled and local drug delivery. *Adv. Healthc. Mater.* 10 (1), 2001341.

HB, N., Bakliwal, S., Pawar, S., 2010. In-situ gel: new trends in controlled and sustained drug delivery system. Int. J. PharmTech Res.2 (2), 1398-408; (b) Jamal, A., Shahzadi, L., Ahtzaz, S., Zahid, S., Chaudhry, A.A., ur Rehman, I., Yar, M., 2018. Identification of anti-cancer potential of doxazocin: loading into chitosan based biodegradable hydrogels for on-site delivery to treat cervical cancer. Mater. Sci. Eng.: C, 82, 102–109.

Kong, Y., Dai, Y., Qi, D., Du, W., Ni, H., Zhang, F., Zhao, H., Shen, Q., Li, M., Fan, Q., 2021. Injectable and thermosensitive liposomal hydrogels for NIR-II light-triggered photothermal-chemo therapy of pancreatic cancer. *ACS Appl. Bio Mater.* 4 (10), 7595–7604.

Huang, D., Zhang, X., Zhao, C., Fu, X., Zhang, W., Kong, W., Zhang, B., Zhao, Y., 2021. Ultrasound-responsive microfluidic microbubbles for combination tumor treatment. *Adv. Therapeut.* 4 (7), 2100050.

Li, J., Zhang, Z., Cao, X., Liu, Y., Chen, Q., 2018. The role of electrostatic repulsion in the gelation of poly (vinyl alcohol)/borax aqueous solutions. *Soft Matter* 14 (32), 6767–6773.

Gholivand, K., Faraghi, M., Pooyan, M., Babaee, L.S., Malekshah, R.E., Pirastehfar, F., Vahabirad, M., 2023. Anti-cancer activity of new phosphoramide-functionalized graphene oxides: an experimental and theoretical evaluation. *Curr. Med. Chem.* 30 (30), 3486–3503.

Gholivand, K., Mohammadpour, M., Derakhshankhah, H., Samadian, H., Aghaz, F., Malekshah, R.E., Rahmatabadi, S., 2023. Composites based on alginate containing formylphosphazene-crosslinked chitosan and its Cu (II) complex as an antibiotic-free antibacterial hydrogel dressing with enhanced cytocompatibility. Int. J. Biol. Macromol., 127297; (b) Salarizadeh, N.; Aallaei, M.R., Zarei, A., Malekshah, R.E., Molaakbari, E., Farajnezhadi, A., Docking and molecular dynamics simulations of flavonoids as inhibitors of infectious agents: rutin as a coronavirus protease inhibitor. ChemistrySelect, 7 (37), e202202043.

Gholivand, K., Alavinasab Ardebili, S.A., Mohammadpour, M., Eshaghi Malekshah, R., Hasannia, S., Onagh, B., 2022. Preparation and examination of a scaffold based on hydroxylated polyphosphazene for tissue engineering: In vitro and in vivo studies. *J. Appl. Polym. Sci.* 139 (20), 52179.

Song, X., Wen, Y., Zhu, J.-L., Zhao, F., Zhang, Z.-X., Li, J., 2016. Thermoresponsive delivery of paclitaxel by β-cyclodextrin-based poly (N-isopropylacrylamide) star polymer via inclusion complexation. *Biomacromolecules* 17 (12), 3957–3963.

Yom-Tov, O., Neufeld, L., Seliktar, D., Bianco-Peled, H., 2014. A novel design of injectable porous hydrogels with in situ pore formation. *Acta Biomater.* 10 (10), 4236–4246.

Haounati, R., Ighnih, H., Ouachtak, H., Malekshah, R.E., Hafid, N., Jada, A., Addi, A.A., 2023. Z-Scheme g-C3N4/Fe3O4/Ag3PO4@ Sep magnetic nanocomposites as heterojunction photocatalysts for green malachite degradation and dynamic molecular studies. *Colloids Surf A Physicochem Eng Asp* 671, 131509.

Ganjali Koli, M., Eshaghi Malekshah, R., Hajiabadi, H., 2023. Insights from molecular dynamics and DFT calculations into the interaction of 1, 4-benzodiazepines with 2-hydroxypropyl-βCD in a theoretical study. *Sci. Rep.* 13 (1), 9866.

Haghbin, M., Malekshah, R.E., Sobhani, M., Izadi, Z., Haghshenas, B., Ghasemi, M., Kalani, B.S., Samadian, H., 2023. Fabrication and characterization of Persian gum-based hydrogel loaded with gentamicin-loaded natural zeolite: an in vitro and in silico study. *Int. J. Biol. Macromol.* 123766.

Choi, S.G., Lee, S.-E., Kang, B.-S., Ng, C.L., Davaa, E., Park, J.-S., 2014. Thermosensitive and mucoadhesive sol-gel composites of paclitaxel/dimethyl-β-cyclodextrin for buccal delivery. *PLoS One* 9 (10), e109090.

Rachmawati, H., Edityaningrum, C.A., Mauludin, R., 2013. Molecular inclusion complex of curcumin–β-cyclodextrin nanoparticle to enhance curcumin skin permeability from hydrophilic matrix gel. *AAPS PharmSciTech* 14, 1303–1312.

Ye, Y.-J., Wang, Y., Lou, K.-Y., Chen, Y.-Z., Chen, R., Gao, F., 2015. The preparation, characterization, and pharmacokinetic studies of chitosan nanoparticles loaded with paclitaxel/dimethyl-β-cyclodextrin inclusion complexes. *Int. J. Nanomed.* 4309–4319.

Huang, H., Yao, J., Li, L., Zhu, F., Liu, Z., Zeng, X., Yu, X., Huang, Z., 2016. Reinforced polyaniline/polyvinyl alcohol conducting hydrogel from a freezing–thawing method as self-supported electrode for supercapacitors. *J. Mater. Sci.* 51, 8728–8736.

Al-Emam, E., Soenen, H., Caen, J., Janssens, K., 2020. Characterization of polyvinyl alcohol-borax/agarose (PVA-B/AG) double network hydrogel utilized for the cleaning of works of art. *Heritage Science* 8, 1–14.

Domb, A.J., Khan, W., 2020. Biodegradable polymers as drug carrier systems. In Polymeric biomaterials, Crc Press: 2020; pp 153-194.

Li, J., Mooney, D.J., 2016. Designing hydrogels for controlled drug delivery. *Nat. Rev. Mater.* 1 (12), 1–17.

Park, J., Sun, B., Yeo, Y., 2017. Albumin-coated nanocrystals for carrier-free delivery of paclitaxel. *J. Control. Release* 263, 90–101.

Sohn, J.S., Yoon, D.-S., Sohn, J.Y., Park, J.-S., Choi, J.-S., 2017. Development and evaluation of targeting ligands surface modified paclitaxel nanocrystals. *Mater. Sci. Eng. C* 72, 228–237.

Zhang, H., Hu, H., Zhang, H., Dai, W., Wang, X., Wang, X., Zhang, Q., 2015. Effects of PEGylated paclitaxel nanocrystals on breast cancer and its lung metastasis. *Nanoscale* 7 (24), 10790–10800.

Polomska, A., Gauthier, M.A., Leroux, J.C., 2017. In vitro and in vivo evaluation of PEGylated layer-by-layer polyelectrolyte-coated paclitaxel nanocrystals. *Small* 13 (2), 1602066.

Zhao, J., Du, J., Wang, J., An, N., Zhou, K., Hu, X., Dong, Z., Liu, Y., 2021. Folic acid and poly (ethylene glycol) decorated paclitaxel nanocrystals exhibit enhanced stability and breast cancer-targeting capability. *ACS Appl. Mater. Interfaces* 13 (12), 14577–14586.

Choi, J.-S., Park, J.-S., 2016. Effects of paclitaxel nanocrystals surface charge on cell internalization. *Eur. J. Pharm. Sci.* 93, 90–96.

Sharma, S., Verma, A., Pandey, G., Mittapelly, N., Mishra, P.R., 2015. Investigating the role of Pluronic-g-Cationic polyelectrolyte as functional stabilizer for nanocrystals: Impact on Paclitaxel oral bioavailability and tumor growth. *Acta Biomater.* 26, 169–183.

Han, S., Li, X., Zhou, C., Hu, X., Zhou, Y., Jin, Y., Liu, Q., Wang, L., Li, X., Liu, Y., 2020. Further enhancement in intestinal absorption of paclitaxel by using transferrin-modified paclitaxel nanocrystals. *ACS Appl. Bio Mater.* 3 (7), 4684–4695.

Lin, Z., Xu, S., Gao, W., Hu, H., Chen, M., Wang, Y., He, B., Dai, W., Zhang, H., Wang, X., 2016. A comparative investigation between paclitaxel nanoparticle-and nanocrystal-loaded thermosensitive PECT hydrogels for peri-tumoural administration. *Nanoscale* 8 (44), 18782–18791.

Lin, Z., Mei, D., Chen, M., Wang, Y., Chen, X., Wang, Z., He, B., Zhang, H., Wang, X., Dai, W., 2015. A comparative study of thermo-sensitive hydrogels with water-insoluble paclitaxel in molecule, nanocrystal and microcrystal dispersions. *Nanoscale* 7 (36), 14838–14847.

Sun, B., Taha, M.S., Ramsey, B., Torregrosa-Allen, S., Elzey, B.D., Yeo, Y., 2016. Intraperitoneal chemotherapy of ovarian cancer by hydrogel depot of paclitaxel nanocrystals. *J. Control. Release* 235, 91–98.

Zhao, D., Hu, C., Fu, Q., Lv, H., 2021. Combined chemotherapy for triple negative breast cancer treatment by paclitaxel and niclosamide nanocrystals loaded thermosensitive hydrogel. *Eur. J. Pharm. Sci.* 167, 105992.

Chen, Y., Huang, Y., Qin, D., Liu, W., Song, C., Lou, K., Wang, W., Gao, F., 2016. β-cyclodextrin-based inclusion complexation bridged biodegradable self-assembly macromolecular micelle for the delivery of paclitaxel. *PLoS One* 11 (3), e0150877.

Gong, G., Fu, B., Ying, C., Zhu, Z., He, X., Li, Y., Xuan, Q., Huang, Y., Lin, Y., Li, Y., 2018. Targeted delivery of paclitaxel by functionalized selenium nanoparticles for

anticancer therapy through ROS-mediated signaling pathways. *RSC Adv.* 8 (70), 39957–39966.